2018

Expected Limits on the Ocean Acidification Buffering Potential of a Temperate Seagrass Meadow

David A. Koweek

R. C. Zimmerman
Old Dominion University, rzimmerm@odu.edu

Kathryn M. Hewett

Brian Gaylord

Sarah N. Giddings

See next page for additional authors

Original Publication Citation

Koweek, D. A., Zimmerman, R. C., Hewett, K. M., Gaylord, B., Giddings, S. N., Nickols, K. J., . . . Caldeira, K. (2018). Expected limits on the ocean acidification buffering potential of a temperate seagrass meadow. *Ecological Applications, 0*(0), 1-21. doi:10.1002/eap.1771

Ecological Applications, 0(0), 2018, pp. 1–21

Expected limits on the ocean acidification buffering potential of a temperate seagrass meadow

David A. Koweek,[1,9] Richard C. Zimmerman,[2] Kathryn M. Hewett,[3] Brian Gaylord,[3] Sarah N. Giddings,[4] Kerry J. Nickols,[5] Jennifer L. Ruesink,[6] John J. Stachowicz,[7] Yuichiro Takeshita,[8] and Ken Caldeira[1]

[1]*Department of Global Ecology, Carnegie Insitution for Science, 260 Panama Street, Stanford, California 94305 USA*
[2]*Department of Ocean, Earth, and Atmospheric Sciences, Old Dominion University, 4600 Elkhorn Avenue, Norfolk, Virginia 23529 USA*
[3]*Bodega Marine Laboratory, University of California Davis, 2099 Westshore Road, Bodega Bay, California 94923 USA*
[4]*Scripps Institution of Oceanography, University of California San Diego, 9500 Gilman Drive 0206, La Jolla, California 92093 USA*
[5]*Department of Biology, California State University Northridge, 18111 Nordhoff Street, Northridge, California 91330 USA*
[6]*Department of Biology, University of Washington, Box 351800, Seattle, Washington 98195 USA*
[7]*Department of Evolution and Ecology, University of California Davis, Davis, California 95616 USA*
[8]*Monterey Bay Aquarium Research Institute, 7700 Sandholdt Road, Moss Landing, California 95039 USA*

Abstract. Ocean acidification threatens many marine organisms, especially marine calcifiers. The only global-scale solution to ocean acidification remains rapid reduction in CO_2 emissions. Nevertheless, interest in localized mitigation strategies has grown rapidly because of the recognized threat ocean acidification imposes on natural communities, including ones important to humans. Protection of seagrass meadows has been considered as a possible approach for localized mitigation of ocean acidification due to their large standing stocks of organic carbon and high productivity. Yet much work remains to constrain the magnitudes and timescales of potential buffering effects from seagrasses. We developed a biogeochemical box model to better understand the potential for a temperate seagrass meadow to locally mitigate the effects of ocean acidification. Then we parameterized the model using data from Tomales Bay, an inlet on the coast of California, USA which supports a major oyster farming industry. We conducted a series of month-long model simulations to characterize processes that occur during summer and winter. We found that average pH in the seagrass meadows was typically within 0.04 units of the pH of the primary source waters into the meadow, although we did find occasional periods (hours) when seagrass metabolism may modify the pH by up to ±0.2 units. Tidal phasing relative to the diel cycle modulates localized pH buffering within the seagrass meadow such that maximum buffering occurs during periods of the year with midday low tides. Our model results suggest that seagrass metabolism in Tomales Bay would not provide long-term ocean acidification mitigation. However, we emphasize that our model results may not hold in meadows where assumptions about depth-averaged net production and seawater residence time within the seagrass meadow differ from our model assumptions. Our modeling approach provides a framework that is easily adaptable to other seagrass meadows in order to evaluate the extent of their individual buffering capacities. Regardless of their ability to buffer ocean acidification, seagrass meadows maintain many critically important ecosystem goods and services that will be increasingly important as humans increasingly affect coastal ecosystems.

Key words: aquatic vegetation; carbon cycling; carbonate chemistry; estuaries; mitigation; ocean acidification; seagrass; Tomales Bay; Zostera marina.

Introduction

Ocean acidification from anthropogenic carbon dioxide (CO_2) emissions presents a change in ocean chemistry that is unparalleled in magnitude and rate over the last 300 million years (Caldeira and Wickett 2003, Hönisch et al. 2012). Given the widespread evidence for ocean acidification impacts on marine life, especially for calcifying organisms (Kroeker et al. 2010, 2013), and increasing evidence for its effects on broader ecological interactions (Gaylord et al. 2015), interest in mitigation strategies has grown in recent years. Although the only global-scale solution to ocean acidification is rapid reduction in CO_2 emissions, mitigation efforts are also being considered at regional-to-local scales. Indirect mitigation strategies include developing the scientific, regulatory, and management frameworks to reduce risk from ocean acidification (e.g., reducing nutrient inputs which drive eutrophication and contribute to coastal acidification through remineralization of organic matter; Strong et al. 2014, Chan et al. 2016, Weisberg et al. 2016). Direct mitigation strategies, in contrast, seek to alter the seawater carbonate chemistry, thereby directly buffering against ocean acidification (Rau 2009, Ilyina et al. 2013, Feng et al. 2016, Koweek et al. 2016). Restoration and protection of seagrass has received particular attention as a possible direct mitigation strategy for protecting coastal ecosystems from ocean acidification. Seagrass beds are highly productive (Unsworth et al. 2012), can reduce water velocity (Fonseca et al. 1982), sequester organic carbon in local sediments (Duarte et al. 2010, 2013), and can export organic carbon to the deep ocean (Duarte and Krause-Jensen 2017). A simple model based on published net production rates from Indo-Pacific tropical seagrasses suggests that tropical seagrasses may be able to alter seawater carbonate chemistry at the local scale (Unsworth et al. 2012). However, this ability has not been quantified with respect to key factors (e.g., plant density, diel cycle

Manuscript received 28 September 2017; revised 6 April 2018; accepted 11 June 2018. Corresponding Editor: Stephen Baines.
[9] E-mail: dkoweek@carnegiescience.edu

variability, seasonal variations in environmental conditions, time-varying water depth, and flow in the meadow) required to translate this idea into a practical management tool.

The west coast of North America presents an ideal environment to investigate the potential of seagrass communities to modify their local carbonate chemistry and ameliorate ocean acidification of the surrounding water. *Zostera marina* (commonly called eelgrass) is widely distributed as mostly isolated patches (2–5 ha) within the small bays and estuaries that dot the Pacific coast of North America (Green and Short 2003). *Z. marina* photosynthesis is stimulated by high CO_2, potentially enhancing the ability of the species to remove CO_2 from the water (Zimmerman et al. 1997, Invers et al. 2001, Palacios and Zimmerman 2007). The California Current System, to which these numerous estuaries and bays open, is already experiencing the chemical and biological impacts of ocean acidification (Gruber et al. 2012, Feely et al. 2016), including impacts on commercially important marine species (e.g., shellfish; Barton et al. 2012). Anticipated impacts to human population centers reliant upon these marine resources are just starting to be understood (Ekstrom et al. 2015).

We developed a biogeochemical box model to explore the capacity of eelgrass to provide localized mitigation of ocean acidification on diurnal-to-monthly timescales. We then parameterized this generalized model for Tomales Bay, California and the *Z. marina* that inhabits the shallow areas of the bay. Building on the earlier work of Unsworth et al. (2012), our model includes the effects of plant density, flow rate, water depth, seasonal variations in water temperature, water column optical transparency, and solar insolation on seagrass metabolism, which result in changes to the carbonate chemistry of the overlying water. In the following sections, we present the model and the empirical parameterizations. Then we discuss steady-state and time-varying model results. Finally, we summarize the insights from the model simulations and consider the model limitations as well as the conditions which may enhance ocean acidification buffering by seagrass meadows. While our model is parameterized for a temperate eelgrass meadow, the approach used here may be applied to any coastal systems, such as kelp forests and coral reefs, to examine the effects of water motion, production, and respiration on seawater carbonate chemistry.

Methods

Model equations

Our model calculates the time-varying changes in seawater carbonate chemistry for a temperate seagrass meadow using spatially implicit advection–reaction equations for the concentrations of dissolved inorganic carbon (DIC) and total alkalinity (TA; both in units of μmol/kg) specified as

$$\frac{d\mathrm{DIC}(t)}{dt} = \frac{u(t)}{L}(\mathrm{DIC}_{\mathrm{in}}(t) - \mathrm{DIC}(t)) - \frac{P_{\mathrm{g}}(t) - R(t)}{\rho h(t)} \quad (1)$$

$$\frac{d\mathrm{TA}(t)}{dt} = \frac{u(t)}{L}(\mathrm{TA}_{\mathrm{in}}(t) - \mathrm{TA}(t)) + \frac{R_{\mathrm{TA}}(P_{\mathrm{g}}(t) - R(t))}{\rho h(t)} \quad (2)$$

where $u(t)$ is the water velocity entering the box as a function of time, and is represented as the sum of mean flow and tidal components, L is the box length (set to 300 m, the median length of eelgrass meadows in upper Tomales Bay; see *Tomales Bay: site characteristics*), $\mathrm{DIC}_{\mathrm{in}}$ and $\mathrm{TA}_{\mathrm{in}}$ are the concentrations of DIC and TA entering the box (also in units of μmol/kg), $P_{\mathrm{g}}(t)$ is gross production by eelgrass per unit area, $R(t)$ is the corresponding eelgrass respiration per unit area, ρ is the seawater density, R_{TA} is the ratio of TA production to organic matter formation due to proton uptake (16/117; Brewer et al. 1975), and $h(t)$ is the tidally varying water depth drawn from tidal predictions within Tomales Bay (see Appendix S1).

Flow representation.—We modeled flow into the box as a combination of mean and tidal flow, such that $u(t) = \bar{u} + u_{\mathrm{tidal}}(t)$, with landward velocities positive and seaward velocities negative. Time-averaged mean velocity, $\bar{u}$, was set -0.01 or -0.05 m/s because this bounds most of the range of mean observed seagrass bed velocities (Appendix S1: Table S1). Tidal velocity, $u_{\mathrm{tidal}}(t)$, was modeled as a function of water depth. We assumed negative (seaward) depth-averaged mean flow in our shallow eelgrass meadow due to the typical lateral structure of mean estuarine circulation in positive estuaries (ocean water is denser than estuarine water), which feature net landward flow in deeper regions and net seaward flow in shallower regions (Geyer and Maccready 2014). While portions of inner Tomales Bay become hypersaline in the fall, much of the Bay maintains a positive density gradient throughout summer months due to solar heating (a "thermal estuary"; Largier et al. 1996), justifying assumptions of net seaward flow along the banks of the estuary where eelgrass meadows are found.

We modeled tidal flow, $u_{\mathrm{tidal}}(t)$, as a function of the changes in water depth, $u_{\mathrm{tidal}}(t) = \alpha\, dh(t + \phi)/dt$ where α is a dimensionless coefficient proportional to the magnitude of the mean velocity ($\alpha = 2 \times 10^{-4}\,|\bar{u}|$). Values of α were not chosen to represent a particular physical relationship between tidal flow and mean flow, but rather were chosen in a simple effort to generate reversible mean flows (i.e., both $u(t) > 0$ and $u(t) < 0$) with a range in tidal velocity approximately four times as great as the magnitude of the time-averaged mean velocity ($\bar{u}$). We represented the phase lag between the tidal flow and changes in water depth with ϕ. We used $\phi = 0$ h to represent a standing wave and $\phi = -3$ h to represent a progressive wave.

Boundary chemistry and model configurations.—Boundary condition water chemistry, $\mathrm{DIC}_{\mathrm{in}}$, and $\mathrm{TA}_{\mathrm{in}}$, were simulated using both estuarine and oceanic estimates based on observations from Tomales Bay and adjacent coastal waters (Smith and Hollibaugh 1997, Feely et al. 2016). In order to gain insight into how hydrodynamic conditions affect eelgrass buffering potential, we considered two sets of boundary conditions. In the first model configuration, we held the oceanic ($\mathrm{DIC}_{\mathrm{ocean}}$ and $\mathrm{TA}_{\mathrm{ocean}}$) and the estuarine ($\mathrm{DIC}_{\mathrm{estuary}}$ and $\mathrm{TA}_{\mathrm{estuary}}$) boundary conditions constant (henceforth referred to as "fixed boundaries"). This model setup simulated an eelgrass meadow where the oceanic and estuarine reservoir volumes on each side of the eelgrass meadow "box" are large relative to the volume of water above the meadow (i.e., "inside the box"). The fixed boundaries setup simulated a condition where any biogeochemical modification of seawater within the meadow does not affect the boundary

reservoirs. Under these fixed boundaries, during a flood tide oceanic waters were advected into the box, and on an ebb tide estuarine waters were advected into the box (Fig. 1).

In the second model configuration, we allowed the eelgrass meadow to exchange water with an oceanic side box and an estuarine side box of equal volume to the eelgrass meadow (subscripts *os* and *es*, respectively, henceforth referred to as "side boxes"). The side boxes configuration was set up to simulate conditions where the water that passes over the eelgrass meadow does not come from infinitely large reservoirs on the

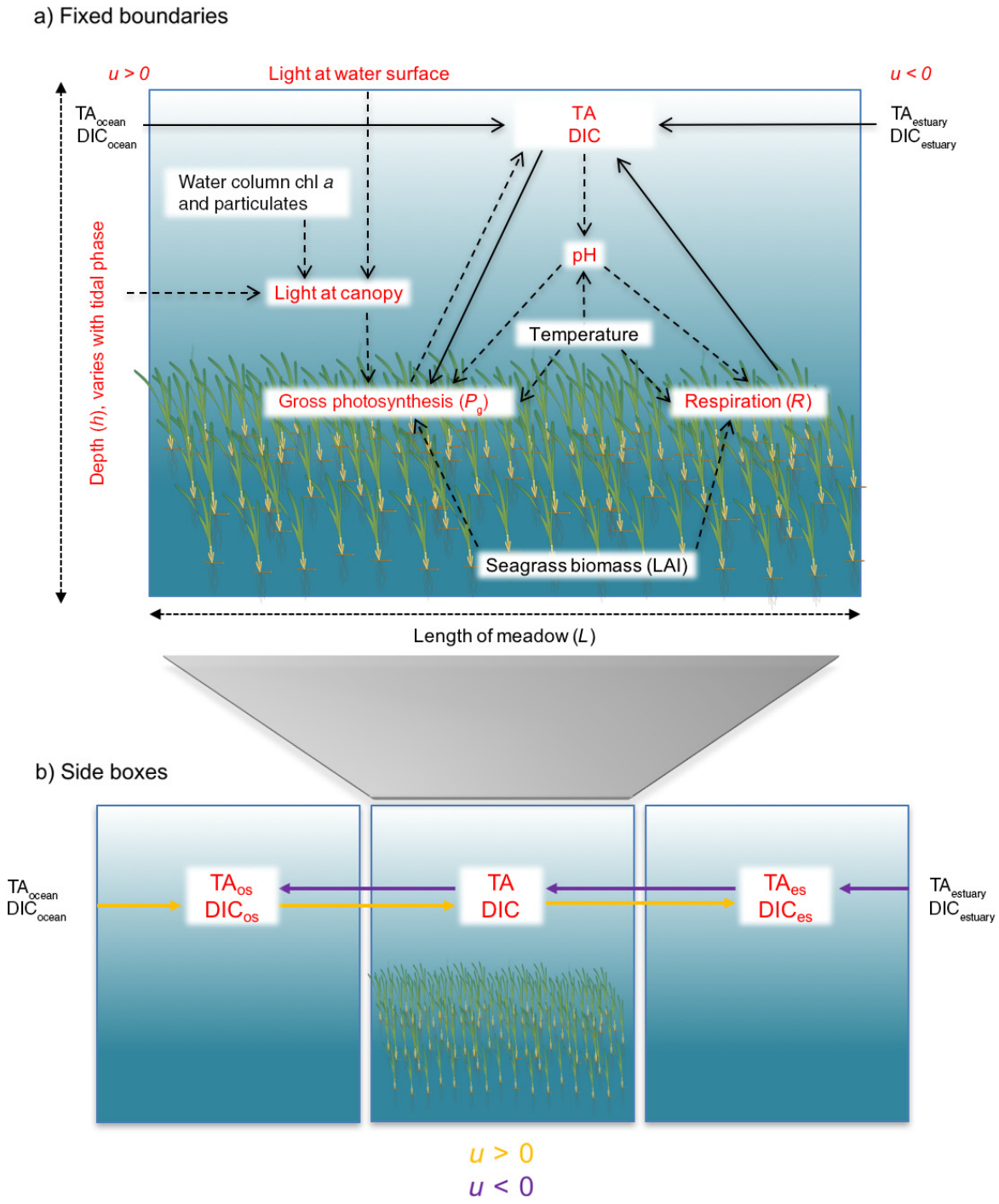

FIG. 1. Schematic of model for (a) fixed boundaries and (b) side boxes configurations. In the fixed boundaries configuration, red font shows simulated variables during a model run, black font shows parameters held fixed in a given model simulation, dotted arrows show the spatial dimensions of the eelgrass meadow, dashed arrows show the directional effects of model parameters and simulated variables on each other, and solid arrows show fluxes of DIC and TA due to advection and metabolism. Panel b) illustrates how the eelgrass box operates within a three-box domain that includes the ocean-side and estuarine-side boxes. Note that the side box concentrations of DIC and TA are shown in red font as well, indicating that they are also simulated model variables.

sides of the meadow, but instead, finite volumes of water subject to modification themselves via advection from the eelgrass meadow. This model configuration provides a middle ground between the fixed-boundaries configuration, where the carbonate chemistry of the oceanic and estuarine reservoirs is fixed, and a closed system without advection where all water chemistry changes in the eelgrass meadow box come from photosynthesis and respiration.

The mass balance equations for the meadow, the estuarine side box, and the oceanic side box were specified as

$$\left.\begin{aligned}
\frac{d\mathrm{DIC}(t)}{dt} &= \frac{u(t)}{L}(\mathrm{DIC}_{\mathrm{os}}(t)-\mathrm{DIC}(t)) - \frac{P_{\mathrm{g}}(t)-R(t)}{\rho h(t)}\\
\frac{d\mathrm{TA}(t)}{dt} &= \frac{u(t)}{L}(\mathrm{TA}_{\mathrm{os}}(t)-\mathrm{TA}(t)) + \frac{R_{\mathrm{TA}}(P_{\mathrm{g}}(t)-R(t))}{\rho h(t)}\\
\frac{d\mathrm{DIC}_{\mathrm{es}}(t)}{dt} &= \frac{u(t)}{L}(\mathrm{DIC}(t)-\mathrm{DIC}_{\mathrm{es}}(t))\\
\frac{d\mathrm{TA}_{\mathrm{es}}(t)}{dt} &= \frac{u(t)}{L}(\mathrm{TA}(t)-\mathrm{TA}_{\mathrm{es}}(t))\\
\frac{d\mathrm{DIC}_{\mathrm{os}}(t)}{dt} &= \frac{u(t)}{L}(\mathrm{DIC}_{\mathrm{ocean}}-\mathrm{DIC}_{\mathrm{os}}(t))\\
\frac{d\mathrm{TA}_{\mathrm{os}}(t)}{dt} &= \frac{u(t)}{L}(\mathrm{TA}_{\mathrm{ocean}}-\mathrm{TA}_{\mathrm{os}}(t))
\end{aligned}\right\} u(t)>0$$

$$\left.\begin{aligned}
\frac{d\mathrm{DIC}(t)}{dt} &= \frac{u(t)}{L}(\mathrm{DIC}_{\mathrm{es}}(t)-\mathrm{DIC}(t)) - \frac{P_{\mathrm{g}}(t)-R(t)}{\rho h(t)}\\
\frac{d\mathrm{TA}(t)}{dt} &= \frac{u(t)}{L}(\mathrm{TA}_{\mathrm{es}}(t)-\mathrm{TA}(t)) + \frac{R_{\mathrm{TA}}(P_{\mathrm{g}}(t)-R(t))}{\rho h(t)}\\
\frac{d\mathrm{DIC}_{\mathrm{es}}(t)}{dt} &= \frac{u(t)}{L}(\mathrm{DIC}_{\mathrm{estuary}}-\mathrm{DIC}_{\mathrm{es}}(t))\\
\frac{d\mathrm{TA}_{\mathrm{es}}(t)}{dt} &= \frac{u(t)}{L}(\mathrm{TA}_{\mathrm{estuary}}-\mathrm{TA}_{\mathrm{es}}(t))\\
\frac{d\mathrm{DIC}_{\mathrm{os}}(t)}{dt} &= \frac{u(t)}{L}(\mathrm{DIC}(t)-\mathrm{DIC}_{\mathrm{os}}(t))\\
\frac{d\mathrm{TA}_{\mathrm{os}}(t)}{dt} &= \frac{u(t)}{L}(\mathrm{TA}(t)-\mathrm{TA}_{\mathrm{os}}(t))
\end{aligned}\right\} u(t)<0 \qquad (3)$$

The mass balance equations for the side boxes describe advective fluxes from both boundaries (depending on flow directionality) and are analogous to the advective flux terms on the DIC and TA mass balances for the eelgrass meadow box. We did not consider any carbon fluxes from localized production in the side boxes (represented in Fig. 1b by the absence of eelgrass within the side boxes). When water flows from the ocean to the estuary ($u(t) > 0$), water within the oceanic side box advects into the meadow box and the meadow box advects its biogeochemically modified water into the estuarine side box. When flow reverses such that water flows from the estuary to the ocean ($u(t) < 0$), water within the estuarine side box advects into the meadow box and the meadow box advects its biogeochemically modified water to the oceanic side box. In recognition that the side boxes themselves are affected by advection from both boundaries, we decided to advect the static estuarine and oceanic reservoirs into the respective side boxes depending upon flow directionality (i.e., $\mathrm{DIC}_{\mathrm{ocean}}$ and $\mathrm{TA}_{\mathrm{ocean}}$ advect into the oceanic side box when $u(t) > 0$; $\mathrm{DIC}_{\mathrm{estuary}}$ and $\mathrm{TA}_{\mathrm{estuary}}$ advect into the estuarine side box when $u(t) < 0$). Note that when $u(t) < 0$, we used $|u(t)|$ in the advection–reaction equations so that the concentration gradient can always be presented as incoming-outgoing.

Photosynthesis and respiration rates.—Vertically integrated rates of gross photosynthesis, P_{g}, and respiration, R, by the eelgrass population were parameterized as functions of eelgrass abundance, downwelling irradiance, and carbonate chemistry based on a series of model simulations calibrated for Tomales Bay using the seagrass bio-optical model GrassLight (Zimmerman et al. 2015). We approximated eelgrass abundance using one-sided leaf area index (LAI = m^2 leaf/m^2 seafloor) because it provides a strong linkage between leaf optical properties and biomass-specific metabolic rates (Zimmerman 2006). Incoming solar irradiance at the top of the eelgrass canopy was modeled based on modeled incoming solar irradiance at the water's surface and the light attenuation coefficient, K_{d}, specific to the bio-optical properties of Tomales Bay (see Appendix S1 for additional information on the solar irradiance and K_{d} calculations). We modeled the vertical distribution of eelgrass leaf biomass within the canopy as a sigmoidal function of height to a distance of 1 m above the seafloor, with leaves oriented 15° from the vertical (Zimmerman 2003), such that the realized canopy height was 0.97 m. When water depth was less than the eelgrass canopy height, the fraction of the eelgrass canopy above the water was presumed to float at the water's surface. Details on the dependence of P_{g} and R on carbonate chemistry within the meadow can be found in Appendix S1.

Since the goal of this study is to evaluate and quantify the buffering potential offered by eelgrass, metabolic rates are for the eelgrass only and do not include contributions from other benthic or water column processes (see *Discussion* for more details). The partial dependence of P_{g} and R on carbonate chemistry leads to coupling between the eelgrass metabolism and overlying water chemistry such that eelgrass metabolism is a function of the overlying water chemistry and the overlying water chemistry is a function of eelgrass metabolism. Details on the metabolic rate parameterizations are provided in Appendix S1.

Other carbon fluxes.—We did not include net calcification (precipitation minus dissolution of calcium carbonate) in our mass balances for DIC and TA because it is not typically a biogeochemically important process in Tomales Bay (Smith et al. 1991). Since TA biogeochemical modification within the meadow is controlled only by R_{TA} and net organic production (NP = $P_{\mathrm{g}} - R$), local TA modification within the eelgrass meadow is typically small (<20 μmol/kg). However, we retained the TA mass balance in the model for completeness and for portability to other systems. In particular, the model has applicability to tropical systems, where net calcification is an important biogeochemical process. In addition, preliminary calculations showed air/sea gas fluxes to be much smaller than those derived from net metabolism (<1% of $P_{\mathrm{g}} - R$). Air/sea gas fluxes were, therefore, excluded in these mass balance calculations.

Buffering effect (buffering capacity).—We defined the buffering effect, or buffering capacity, as the change in

carbonate chemistry between a control simulation without eelgrass (represented by setting LAI = 0) and a model simulation that contains eelgrass at a given density (represented by LAI > 0). We calculated buffering effects after holding all other model parameters constant (e.g., boundary conditions, season, flow velocity, tidal phasing, etc.) between the control and eelgrass-populated model runs such that the differences in carbonate chemistry are solely attributable to the eelgrass density in the model box.

Model resolution.—Model simulations were run at a 15-min time step in which each time step fully resolves the carbonate chemistry within the meadow (as well as the carbonate chemistry within the side boxes when the model is configured to run with side boxes), along with eelgrass meadow simulated P_g and R. The duration of the model time-step is sufficient to capture intra-day variation in light availability caused by Earth's rotation. But the model does not include weather-scale variation in light availability that results from clouds. The model includes fluctuations in water depth driven by the mixed semi-diurnal tides.

Tomales Bay

Site characteristics.—We chose to parameterize our generalized model for an eelgrass meadow in Tomales Bay, California, USA (Fig. 2). Located north of San Francisco, Tomales Bay is a shallow, highly unidirectional (~20 km long by ~1 km wide) semi-enclosed west coast estuary formed in a drowned rift valley of the San Andreas Fault (Hearn and Largier 1997; Fig. 2a). This coastal region experiences some of the strongest upwelling favorable winds along the west coast of North America (Largier et al. 2006). Fresh water enters the bay from its southern end (Lagunitas Creek) and its eastern side (Walker Creek), mostly during winter months. Waters in Tomales Bay experience a wide range of physical and chemical conditions as newly upwelled water is introduced to the bay and begins to undergo biogeochemical and physical modification. Tomales Bay is the site of a large bivalve aquaculture economy (Dumbauld et al. 2009), so the impacts of ocean acidification are likely to have economic, as well as ecological, ramifications.

Eelgrass meadows in upper Tomales Bay are distributed in about 25 patches between the mouth of the bay and Hog Island, located ~6 km from the mouth of the bay (Fig. 2b). Manual analysis of patch dimensions in upper Tomales Bay using Google Earth Pro[10] revealed median dimensions of 304 m (longest axis) × 38 m (orthogonal axis), with a median patch area of ~1 ha, which covers a total area of about 40 ha. This represents about 10% of the bay area between the mouth and Hog Island.

Seasonal variability.—We conducted a series of 30-d model runs designed to simulate summer upwelling, summer relaxation, and winter non-upwelling conditions at an eelgrass meadow in upper Tomales Bay. Eelgrass meadows in this region experience forcing from both the mouth (oceanic source waters) and head (estuarine source waters) of the bay (Largier et al. 1997, Smith and Hollibaugh 1997). This forcing allowed us to test hypotheses about the effects of the carbonate chemistry of impinging waters on the buffering capacity of the eelgrass meadow. We chose to simulate three seasonal (summer upwelling, summer relaxation, and winter) conditions because they provide maximum contrast in environmental conditions (temperature, salinity, carbonate chemistry, and light) experienced by the eelgrass meadow in Tomales Bay over an annual cycle. We utilized Smith and Hollibaugh's (1997) 8-yr-long bimonthly water column chemistry data set collected in inner-to-middle Tomales Bay to build composite annual cycles of temperature, salinity, and water chemistry, from which we chose our seasonal values. The dates of the seasonal simulations were chosen by selecting the maximum and minimum values for the Bakun Upwelling Index parameterization provided in Smith and Hollibaugh for Tomales Bay (1997), which they used as a proxy for the strength of the annual upwelling cycle. These maxima and minima were Calendar Days 198 and 16, respectively. Therefore summer and winter model simulations started on Calendar Days 183 and 1, respectively.

Selected summer values of pH_{ocean} represent an attempt to bound the range in expected pH along the coast between periods of upwelling and relaxation (Feely et al. 2016). Winter pH_{ocean} was taken as 8.1 to represent the return of offshore California Current waters to the coast in the absence of upwelling (Feely et al. 2016). Values for $pH_{estuary}$ and $TA_{estuary}$ were based on the 8-yr composite record from Smith and Hollibaugh (1997). DIC_{ocean} was calculated from pH_{ocean} and TA_{ocean} and $DIC_{estuary}$ was calculated from $pH_{estuary}$ and $TA_{estuary}$ (see *Model Code* for details on carbonate chemistry calculations). We held TA_{ocean} constant and equal to $TA_{estuary}$ to avoid the confounding influence of advective TA fluxes on our interpretation of the model simulations. Finally, we controlled light attenuation in the water column of the box model using a light attenuation coefficient, K_d, which was parameterized in GrassLight. To parameterize the summer K_d value, we assumed the summer chlorophyll *a* (chl *a*) concentration was 8 μg/L and the total suspended matter (TSM) concentration was 4 mg/L. We assumed the winter chl *a* concentration was 5 μg/L and the TSM concentration was 4 mg/L to parameterize the winter K_d value (see Appendix S1 for more details). Although chl *a* and TSM were used to inform estimates of the bio-optical properties of the water column, they were not used directly in the box model calculations.

We held temperature and salinity, and therefore ρ, constant within each seasonal simulation, only varying them across the seasonal scenarios in accordance with Table 1. We also repeated each simulation four times, varying the phasing of the incoming velocity with respect to the changes in tidal height (ϕ) from 0 to −3 h in order to capture all possible tidal cycle-diel cycle interactions. Results of these four model runs were aggregated to represent a broader distribution of pH modification expected within each modeling scenario (Fig. 3).

Model code

We conducted all box model simulations, data analysis, and plotting in R (R Core Team 2016). We used the deSolve package for the mass balance equations (Soetaert

[10] https://www.google.com/earth/desktop/

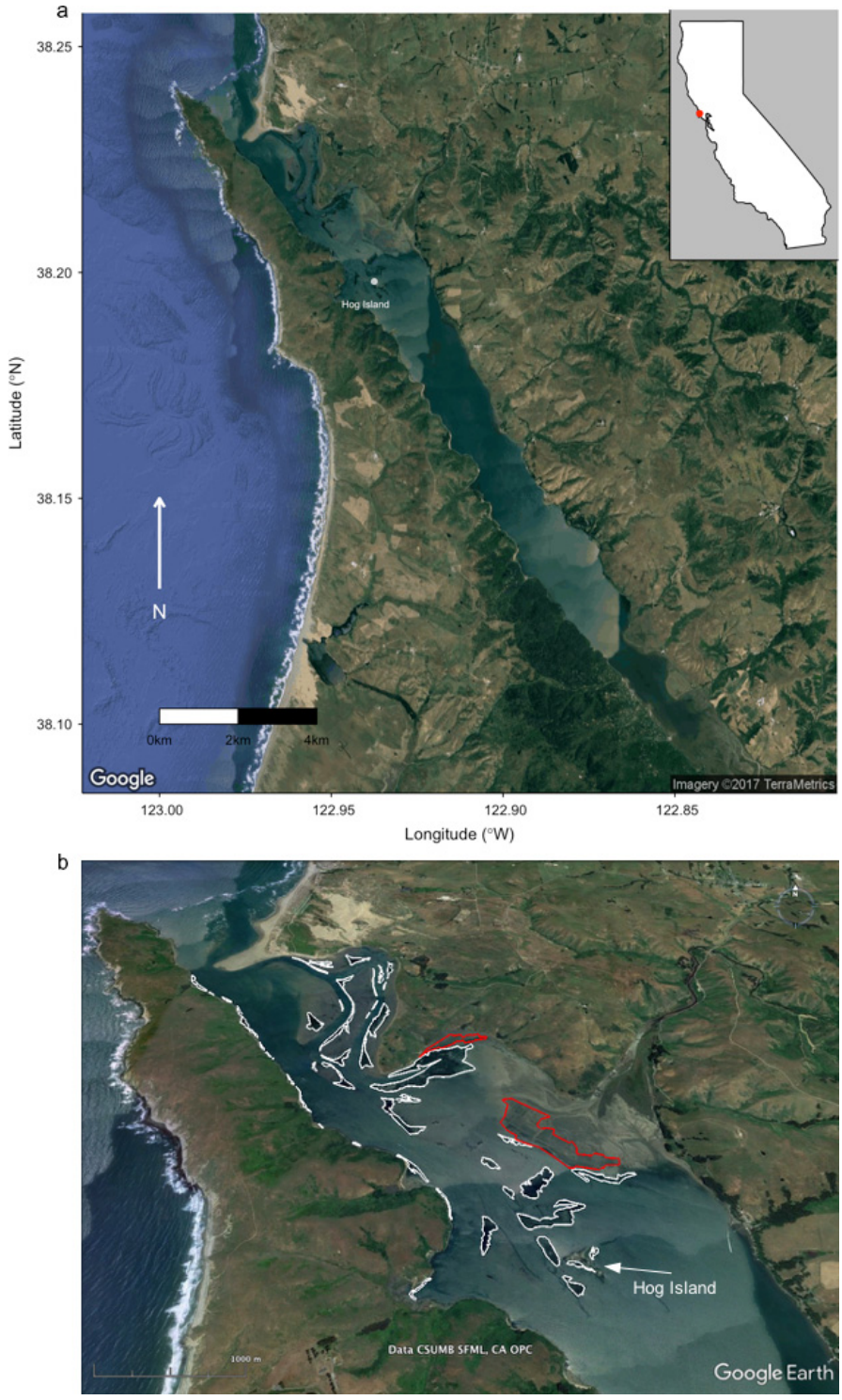

FIG. 2. (a) Map of Tomales Bay, California, USA, taken from Google Earth. Image reveals the narrow, linear nature of this inlet. Eelgrass meadows appear as dark patches near Hog Island (white dot) in the upper one-third of the estuary. Red dot on the inset map indicates the location of Tomales Bay on the coast of California, USA. (b) Zoomed-in image of upper Tomales Bay shows eelgrass meadows outlined in white and oyster aquaculture regions outlined in red.

et al. 2010). We used the seacarb package for all carbonate chemistry calculations with default settings for all equilibrium constants (Gattuso et al. 2016). We assumed negligible pressure effects and contributions from nitrate, silicate, and phosphate in our carbonate chemistry calculations. All figures in the main text and Appendix S1 were developed using the ggplot2 package (Wickham 2009).

TABLE 1. Set of environmental conditions within the eelgrass meadow and boundary water chemistries used to parameterize seasonal simulations.

Season	Start calendar day	T (°C)	Salinity	pH_{ocean}	TA_{ocean}	$pH_{estuary}$	$TA_{estuary}$
Summer (upwelling)	183	18	35	7.7	2,300	8.0	2,300
Summer (relaxation)	183	18	35	8.0	2,300	8.0	2,300
Winter	1	11	28	8.1	2,200	8.2	2,200

Notes: pH is on the total scale. TA is in units of of μmol/kg.

RESULTS

Steady-state insights

We begin by considering the steady-state solution to the eelgrass meadow DIC mass balance ($d\mathrm{DIC}(t)/dt = 0$) since the DIC mass balance is the primary driver of biogeochemical variability in the eelgrass meadow. In this steady-state condition, the advective term (first term on the right side of Eq. 1) and the reactive term (second term on the right side of Eq. 1) are set equal. Therefore the difference in DIC between the incoming and outgoing water across the box can be calculated as

$$\mathrm{DIC_{in}} - \mathrm{DIC} = \frac{L}{\bar{u}\rho h}\mathrm{NP} \tag{4}$$

where NP is net primary production, $\mathrm{NP} = P_g - R$. This steady-state solution, which is essentially equivalent to Unsworth's simple model (2012), can provide several important insights. First, $\mathrm{DIC_{in}} - \mathrm{DIC}$ (ΔDIC, i.e., the change in DIC from the water that enters the box to the water that leaves the box) is proportional to the seawater residence time in the eelgrass meadow, $\tau = L/\bar{u}$. Second, ΔDIC is inversely proportional to the water depth, h, over the eelgrass. Third, ΔDIC is proportional to the net production, NP.

We converted ΔDIC to ΔpH because of its familiarity to many readers using the summer temperature (18°C), salinity (35), and TA (2,300 μmol/kg) for the meadow from Table 1. The steady-state results (Fig. 4) show that the greatest potential for pH buffering of incoming seawater chemistry lies in an ecosystem with long residence time and high depth-averaged net production (upper right-hand corner of Fig. 4a, b). The dashed lines on Fig. 4a, b display the residence times for flow velocities of 0.01 and 0.05 m/s through a meadow of length L = 300 m. Fig. 4a, b also demonstrate the non-linear dependence of pH on DIC such that the same depth-averaged net production produces larger pH buffering when the starting pH is lower. When the starting pH is set to 7.7 (Fig. 4a), the same depth-averaged production integrated over the same residence time yields a greater ΔpH than when the starting pH is set to 8 (Fig. 4b).

The steady-state approximations shown in Fig. 4 are adequate for short residence times in tidally driven coastal regions where one can consider the depth overlying the meadow constant over small periods of time. However, steady-state assumptions over short timescales (i.e., <1 h) do not hold at the longer residence times (>3 h) necessary to achieve large biogeochemical modification in steady-state conditions. At these longer time scales, tidal fluctuations and subsequent interactions with downwelling irradiance and, therefore, benthic metabolism, combine to produce a more complex set of biogeochemical conditions.

Box model simulations

Relaxing the static assumptions of the steady-state calculations allowed us to investigate more realistically the potential of eelgrass to buffer the chemistry of water advected into the meadow. We continue to use pH as the carbonate chemistry variable from which we consider buffering potential, but note that the model could be used to conduct a similar set of analyses on other carbonate system parameters of interest (e.g. $\Omega_{\mathrm{Aragonite}}$ or pCO_2).

Summer upwelling results.—Summer upwelling model experiments showed that the pH in the eelgrass meadow was close to the pH of the estuary, which served as the primary source water because mean flow was seaward (Fig. 5). In our fixed boundary simulations, the median pH in the eelgrass meadow was highly consistent across all LAI and flow velocity conditions, ranging from 7.98 to 8.007 (Fig. 5a). The low flow conditions ($\bar{u}$ = −0.01 m/s) had occasional periods where pH was elevated above 8.1; the high flow simulations ($\bar{u}$ = −0.05 m/s) reached maximum pH values between 8.05 and 8.1 (Fig. 5a). Minimum pH across the LAI and flow velocity conditions ranged from 7.637 to 7.7 (Fig. 5a). Values below 7.7 reflect a combination of nighttime respiration and advection of low pH ocean water into the eelgrass meadow.

Buffering effects for the fixed boundaries simulations were greater at lower flow as expected (Fig. 5b). Median buffering effects in the low flow simulations started at 0.018 for LAI = 1 and increased to between 0.034 and 0.037 for LAI values between 3 and 5. Median buffering in the high flow simulations ranged from 0.005 to 0.011 across LAI = 1–5. Both maximum and minimum buffering scaled with LAI. In our discussion of maximum and minimum buffering, we focus on the low flow simulations because they provide a greater range of buffering effect estimates than do the high flow simulations due to the greater residence time in the eelgrass meadow. Maximum buffering effects ranged from 0.054 at LAI = 1 to 0.143 at LAI = 5. Similarly minimum buffering range from −0.037 at LAI = 1 to −0.207 at LAI = 5. Note that the magnitude of negative buffering (i.e., ΔpH < 0) was greater than the positive buffering at high LAI.

The side boxes upwelling simulations generated qualitatively similar pH distributions (Fig. 5c) and buffering effects to the fixed boundaries simulation (Fig. 5d). However, we did notice one important difference between side boxes and fixed boundaries simulations. Incorporation of repeated

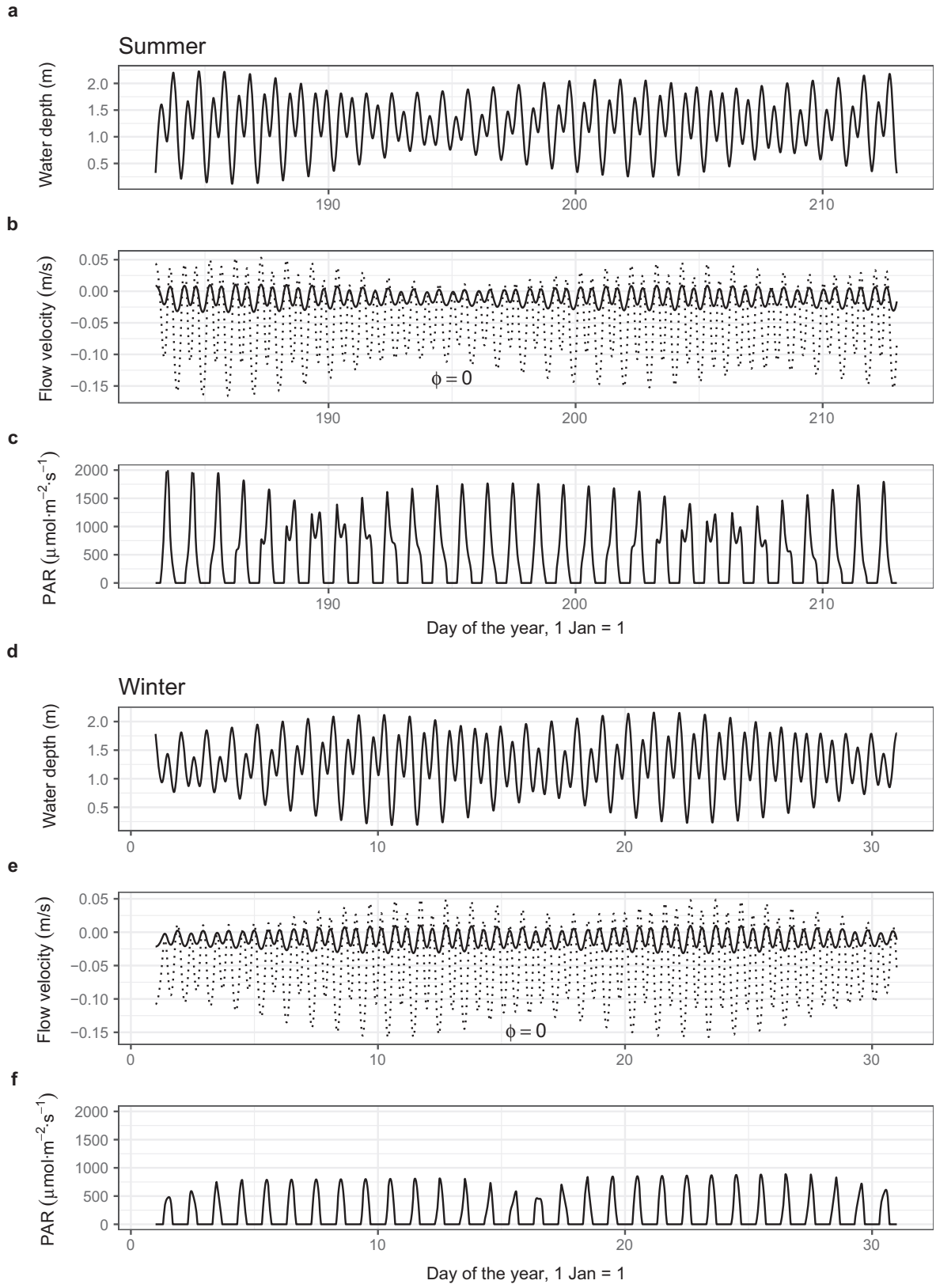

FIG. 3. (a, d) Water depth, (b, e) velocity, and (c, f) solar irradiance (photosynthetically available radiation, PAR) at the top of the eelgrass canopy for summer (a–c) and winter (d–f) modeling scenarios. Solid lines in panels b) and e) show velocity time series for $\bar{u} = -0.01$ m/s and dotted lines in panels b) and e) show velocity time series for $\bar{u} = -0.05$ m/s. The phase shift, ϕ, is expressed in hours.

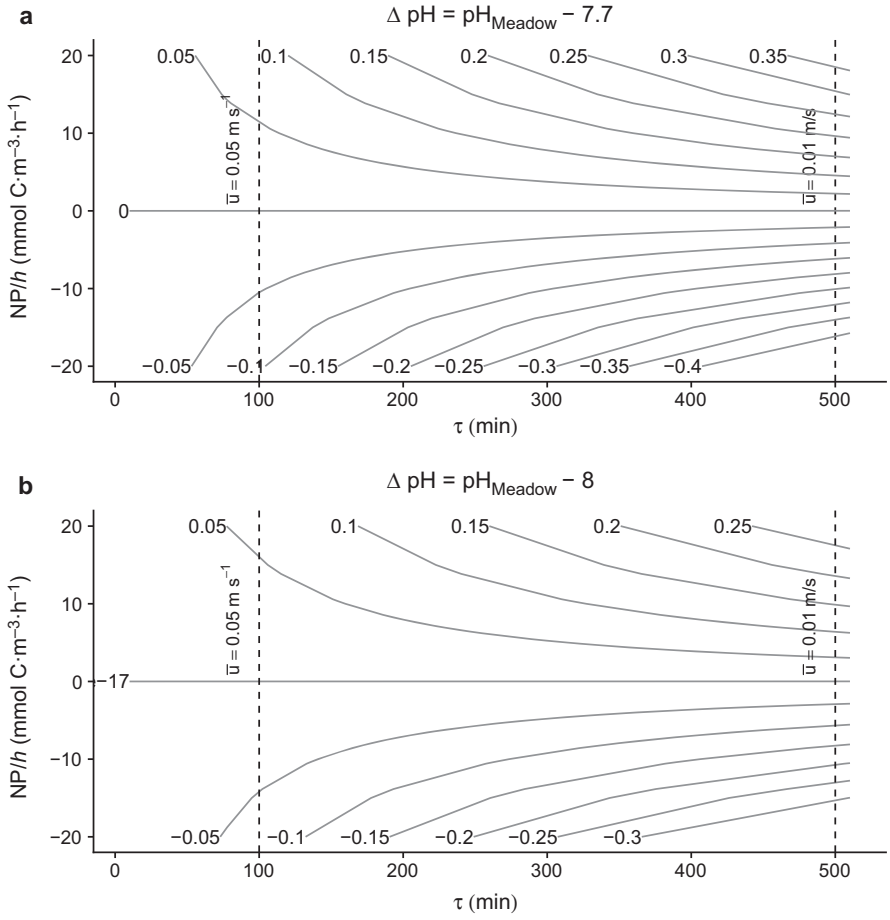

FIG. 4. Steady-state buffering effects from (a) pH = 7.7 (pH_{ocean} in summer upwelling simulations) and (b) pH = 8.0 (pH_{ocean} in summer relaxation simulations) as functions of water residence time within the eelgrass meadow, τ, and depth-averaged net primary production.

"sloshing" increased the median pH across all LAIs (including LAI = 0) and flow conditions as compared to the same conditions in the fixed boundaries simulations. The effect of sloshing on median pH ranged from 0.004 to 0.024. Despite the effect of increasing the median pH, sloshing had a near negligible effect on buffering capacity. The maximum increase in buffering capacity from the repeated "sloshing" of the side boxes simulations was 0.002. We therefore conclude that sloshing increased the median pH in the meadow primarily by altering the advective fluxes, but had minimal effect on net production, and therefore, buffering capacity within the meadow.

Summer relaxation results.—Summer relaxation simulations showed small, but consistent, increases in pH relative to the incoming water (Fig. 6). In these simulations, both the ocean side and estuary side boundaries were set to pH = 8, therefore deviations from pH = 8 reflect local modification via eelgrass net production. Median pH in the fixed boundaries low flow conditions ranged from 8 to 8.035 (Fig. 6a). Median pH in the fixed boundaries high flow conditions was closer to 8, reflecting the dominance of advection over metabolism in the high flow scenarios. pH maxima and minima scaled with LAI and flow condition such that pH ranges were greatest when mean flow was low and LAI = 5. Side boxes simulations generated pH distributions similar to the fixed boundaries simulations (Fig. 6a, c). This similarity suggests little influence of "sloshing" when the boundary source waters are equivalent.

Buffering effects for the fixed boundaries (Fig. 6b) and side boxes (Fig. 6d) simulations appear similar, and similar to the upwelling simulations (Fig. 5). Buffering effects increase from LAI = 1 to LAI = 3 and then level off such that buffering effects are approximately equal across the range of LAI = 3–5 for both the fixed boundaries and side boxes simulations. Again we focus on the low flow conditions since the greatest ranges in buffering effects are observed in the low flow conditions. Median buffering at LAI = 1 was 0.017 and increased to a maximum of 0.038 units at higher LAI. Maximum buffering in the low flow conditions ranged from 0.051 at LAI = 1 to 0.142 at LAI = 5. Minimum buffering reached −0.203 at LAI = 5. Similar to the upwelling simulations, pH ranges increased with LAI and were greater at low mean flow compared to high mean flow. The buffering effect was also asymmetric around 0 such that the range in negative buffering effects was greater than the range in positive buffering effects (Fig. 6b, d).

Interaction between summer light and density-dependent eelgrass metabolism.—Buffering effects in the summer upwelling and relaxation simulations scaled non-linearly with LAI such that buffering effects increased from LAI = 1–3 and

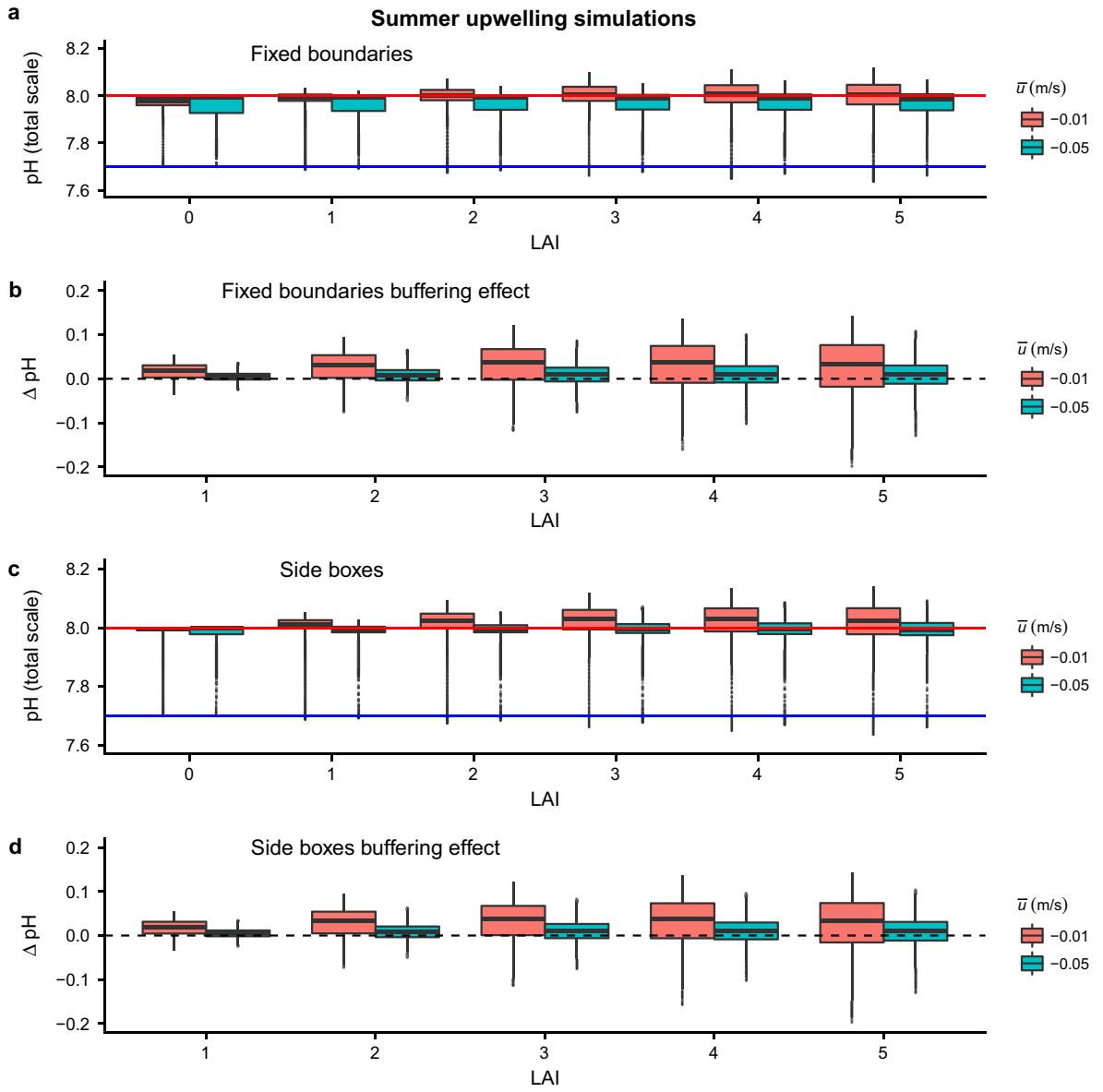

FIG. 5. Summer upwelling model simulation results. (a) Summary boxplots for fixed boundaries simulations, (b) calculated buffering effects for the fixed boundaries simulations, (c) summary boxplots for side boxes simulations, and (d) calculated buffering effects for the side boxes simulations. Each Tukey boxplot shows the aggregation of four model runs, each 30 d in length at 15-min resolution (n = 2,881 observations per model run), where we varied the phasing between the changes in box depth and incoming velocity from 0 to −3 h in the four model runs (n = 11,524 model observations per boxplot). The center line on each Tukey boxplot is the median. The upper and lower hinges are the 75th and 25th percentiles, respectively, which together define the interquartile range (IQR). The upper and lower whiskers extend to the furthest data point up to 1.5 times the IQR beyond the upper and lower hinge, respectively. Outlier data points extending beyond the upper and lower whiskers are plotted individually. In panels a) and c), the red line shows the pH of the estuarine boundary and the blue line shows the pH of the ocean boundary.

then leveled off between LAI = 3–5. We attribute this result to the differing dependence of P_g and R to light and LAI (Fig. 7). Gross production is dependent on light and LAI. Eelgrass at LAI = 1 is light-saturated under low irradiance, but at LAI = 5 has still not reached light saturation at 1,000 μmol·m^{-2}·s^{-1} (Fig. 7a). Unlike P_g, R is light independent and increases linearly as a function of LAI (Fig. 7b). Net production, NP = P_g − R, therefore exhibits non-linear dependence on both light and LAI. At the median light values for the summer simulations (calculated including all day and night times), net production, and therefore buffering capacity, was approximately equal for eelgrass communities of LAIs between 3 and 5. Minimum and maximum pH in the summer simulations, in contrast, scale with LAI (Fig. 7). The plot of net metabolism (Fig. 7c) clearly shows the LAI dependence for negative net metabolism, which occurs because the metabolic demand of the eelgrass, R, outstrips the gross production, P_g, at lower light levels and high densities. In contrast, at the maximum light values simulated during the summer model runs (Fig. 3), the light supply is sufficient to saturate photosynthesis of the densest eelgrass communities simulated here. The high light availability

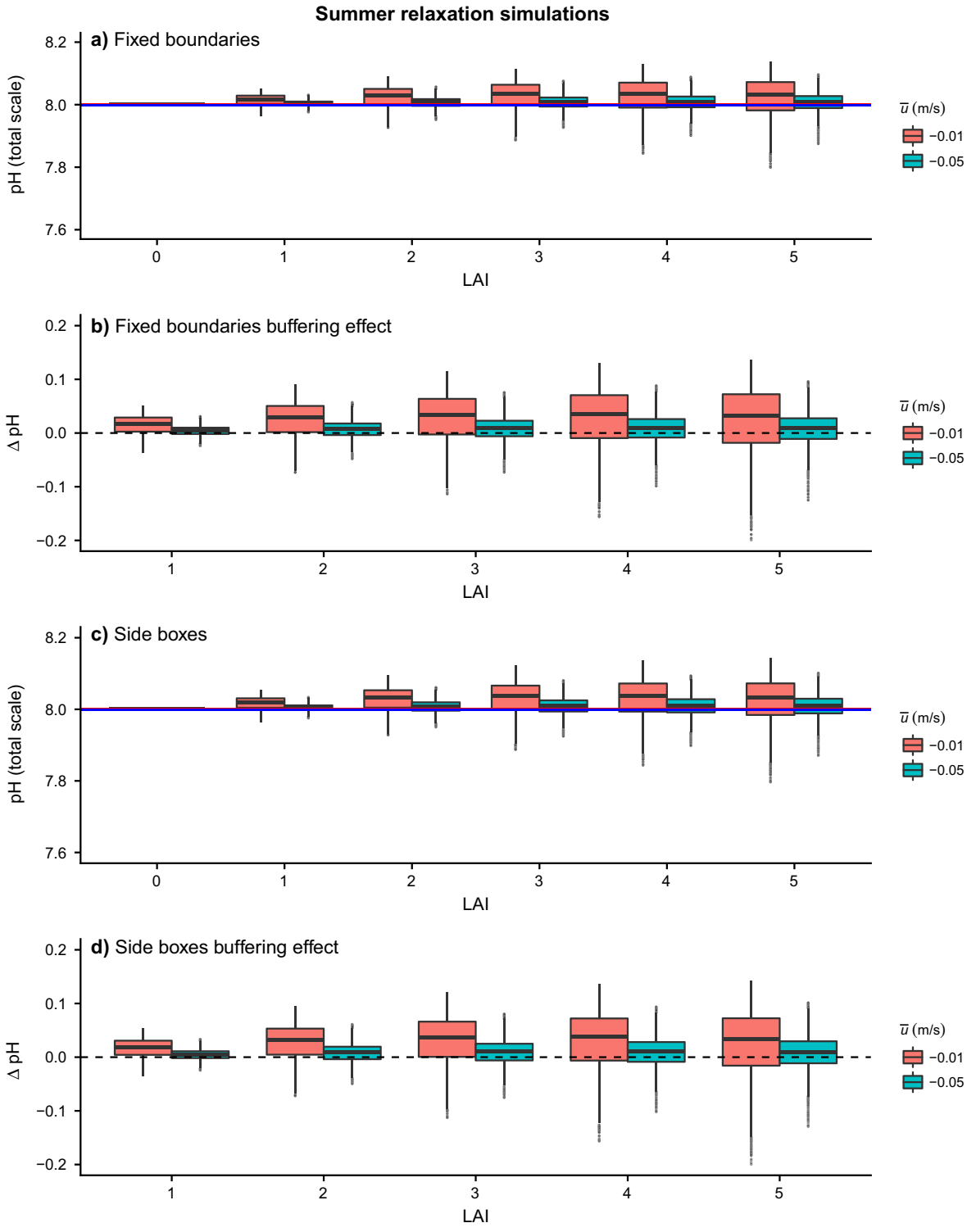

FIG. 6. Summer relaxation model simulation results. (a) Summary boxplots for fixed boundaries simulations, (b) calculated buffering effects for the fixed boundaries simulations, (c) summary boxplots for side boxes simulations, and (d) calculated buffering effects for the side boxes simulations. The description of the boxplot statistics can be found in the Fig. 5 caption. On a) and c), the red line showing the pH of the estuarine boundary and the blue line showing the pH of the ocean boundary are set equal at pH = 8.

results in greatest net production at highest LAI (Fig. 7c). The increased net metabolism as a function of LAI results in LAI-dependent pH buffering such that the greatest pH increases scale with LAI. Although P_g and R are represented in our model as polynomial functions of LAI, pH, and light (see Appendix S1 for more details), these parameterizations were determined through a series of GrassLight simulations which were intended to encapsulate the important

bio-optical processes including self-shading at higher canopy density and biomass-dependent eelgrass respiration. This gives us confidence that our model results and interpretations are representative of integrated ecophysiological processes operating within the eelgrass meadow.

Winter results.—Median pH in the winter scenarios was close to 8.2, the pH of the estuarine margin (the primary source water; Fig. 8). Maximum pH reached 8.406 in the fixed boundaries simulations (Fig. 8a) and 8.417 in the side boxes simulations (Fig. 8c). Minimum pH across all model

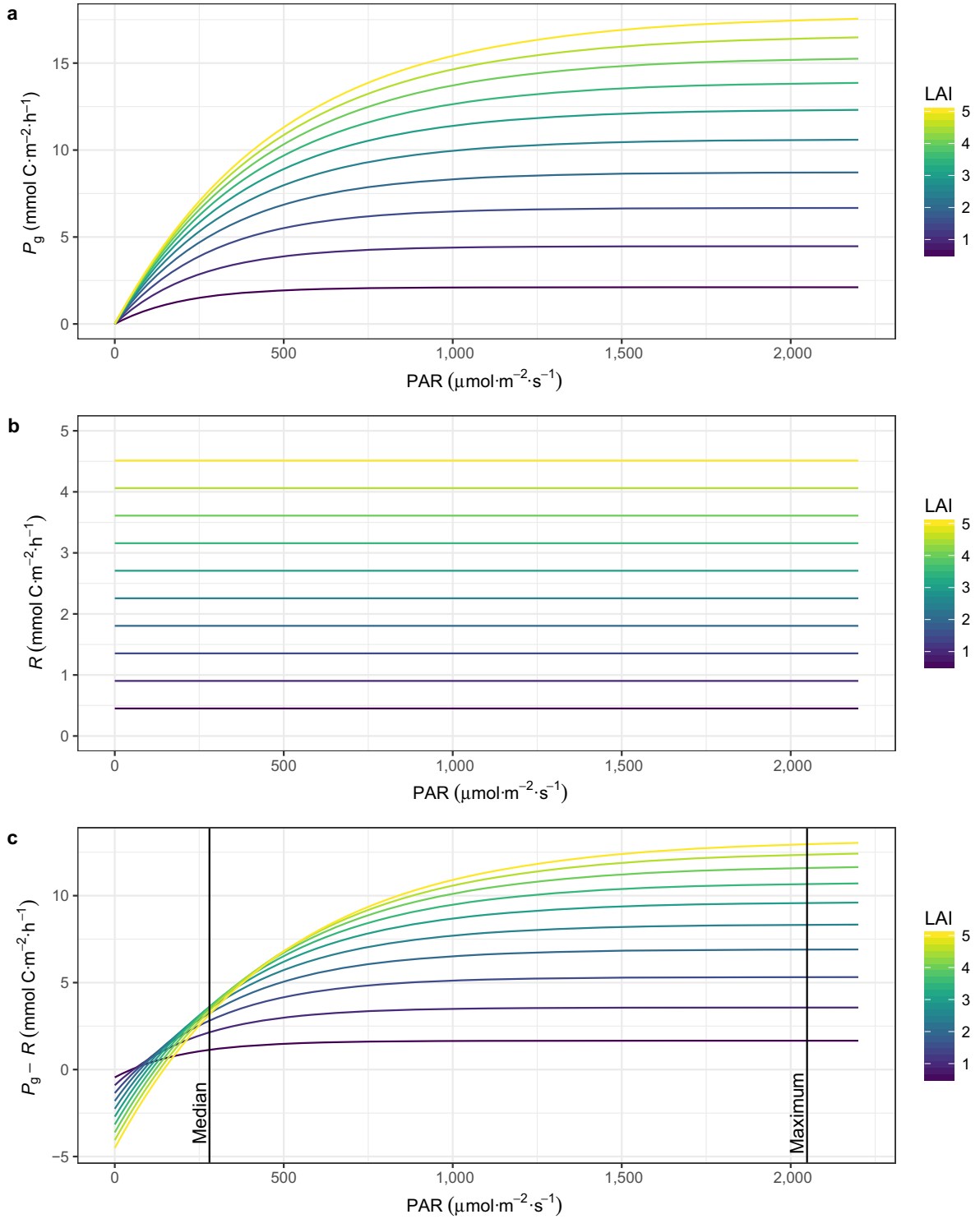

FIG. 7. Summer metabolism–irradiance curves for (a) gross photosynthesis, (b) respiration, and (c) net production as a function of leaf area index (LAI). Metabolic rates were calculated at pH = 8 and total alkalinity = 2,300 µmol/kg. The vertical lines in panel c) show the median and maximum light values at the top of the eelgrass canopy observed over the summer simulations.

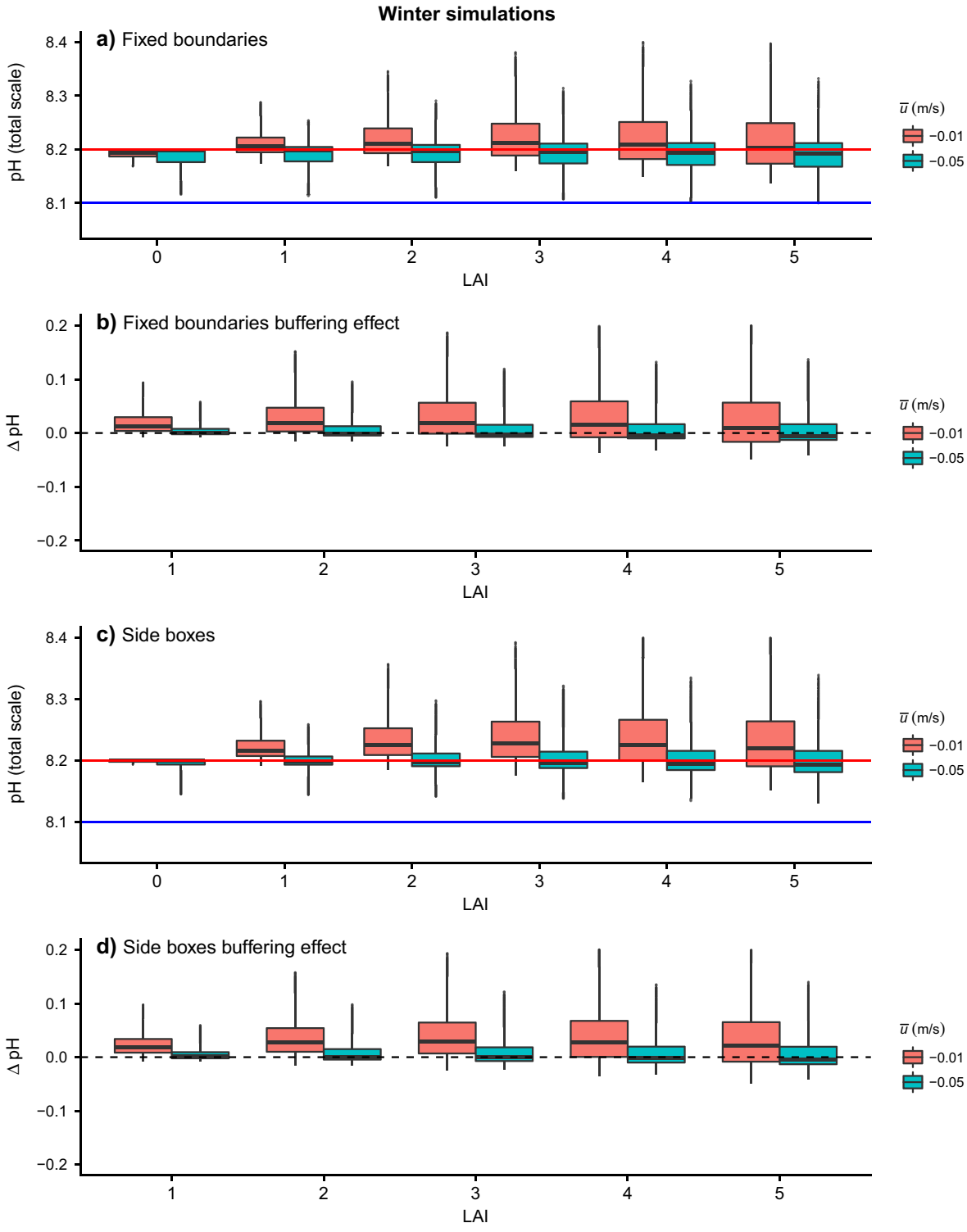

FIG. 8. Winter model simulation results. (a) Summary boxplots for fixed boundaries simulations, (b) calculated buffering effects for the fixed boundaries simulations, (c) summary boxplots for side boxes simulations, and (d) calculated buffering effects for the side boxes simulations. The description of the boxplot statistics can be found in caption for Fig. 5. In panels a) and c), the red line shows the pH of the estuarine boundary and the blue line shows the pH of the ocean boundary.

simulations was 8.1. Median buffering effects for low flow simulations aggregating the fixed boundaries and side boxes configurations were small, but positive, for all LAI values (<0.03 units). Median buffering effects were negligible at high flow conditions across all LAI values and boundary configurations. Maximum buffering effects scaled with LAI and flow conditions (as with summer simulations). However, maximum buffering during winter was larger than during

summer. At LAI = 5, maximum buffering for the fixed boundaries simulations was 0.212 units (Fig. 8b) and for the side boxes simulations was 0.218 (Fig. 8d). Minimum buffering was close to zero for both the fixed boundaries and side boxes simulations. The strong similarity between calculated buffering capacity for the fixed boundaries and side boxes simulations supports the findings of the summer simulations which suggest minimal effects of "sloshing" on buffering capacity.

Median pH dependence on mean velocity.—Our summer and winter model experiment results highlighted the close agreement between median pH and the pH of the primary source waters (the estuarine margin). We conducted a simple model experiment where we changed $\bar{u}$ to test for the effects of mean flow on pH. We found that $\bar{u}$ exerts a dominant control on pH within the eelgrass meadow (Fig. 9). In summer upwelling conditions, when $\bar{u} < 0$ (seaward flow), median pH within the meadow was close to the estuarine value of 8 and when $\bar{u} > 0$ (landward flow), median pH within the meadow approached the oceanic value of 7.7. When $\bar{u} = 0$ (i.e., flow controlled only by tidal velocities), median pH within the eelgrass meadow assumed an intermediate distribution between the estuarine and oceanic end members (except for the winter side boxes simulation which had a median pH above the estuarine end member, but below the condition where $\bar{u} = -0.01$ m/s; Fig. 9b). Simulations with winter conditions produced similar dependence of pH within the meadow on the pH of the primary source water (Fig. 9b). The results of this experiment cannot be explained by variations in tidal velocity, since all three $\bar{u}$ conditions had the same tidal velocity. Nor can they be explained by the starting pH of the model simulations, which was always set to the oceanic pH (7.7 for summer upwelling simulations, 8.1 for winter simulations) for all boxplots shown in Fig. 9. While we believe our selection of negative $\bar{u}$ for these model simulations is justified, we emphasize that deviations from this assumption would lead to different pH ranges in accordance with pH of the source waters from the primary directionality. These results further underscore the importance of advective fluxes of DIC and TA into the meadow relative to metabolic fluxes of DIC and TA within the meadow in exerting control over the pH within the meadow.

Seasonal effects on maximum pH buffering.—Maximum buffering was greater in the winter than in the summer and minimum (negative) buffering was greater in the summer than in the winter. This result seemed counterintuitive since winter

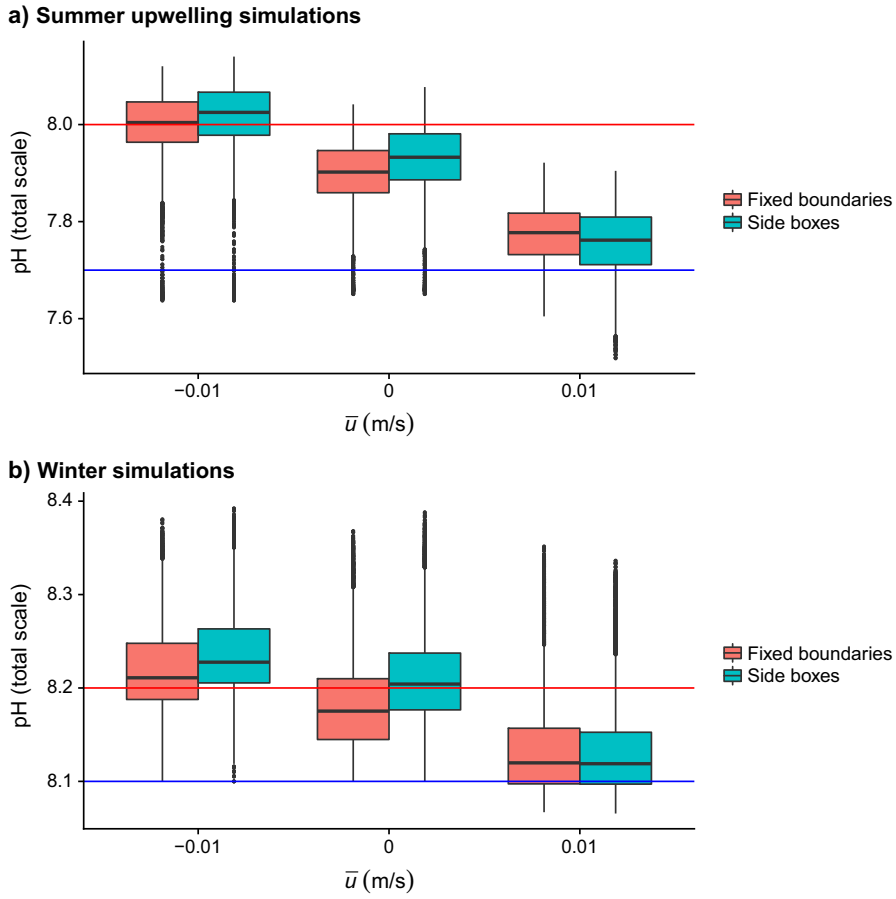

FIG. 9. Effect of varying mean velocity on pH for (a) summer simulations and (b) winter simulations. $\bar{u} < 0$ indicates that the mean velocity goes from the head to the mouth of the estuary and $\bar{u} > 0$ indicates that the mean velocity goes from the mouth to the head of the estuary. On both plots, the red line shows the pH of the estuarine source and the blue line shows the pH of the ocean source. All summer runs were conducted with LAI = 5 and all winter runs were conducted with LAI = 3.

light levels and water temperatures were lower than summer values (Fig. 3 and Table 1). Indeed, maximum and median net production rates were lower in the winter than in the summer (Fig. 10a). Yet the impact of the net production rates on the overlying water chemistry in this model was modulated by the water depth, which controlled light propagation to the eelgrass canopy as well as the volume of water in the meadow box. The summer water depth cycle, constructed from the tidal predictions in Tomales Bay (Fig. 3a), reveals that afternoon water depths, when net production was greatest, were typically >1 m (Fig. 10b). However, afternoon water depths in the winter simulations were often <0.5 m (Figs. 3d, 10c). The resulting effect was that maximum *depth-averaged net production rates* in the winter simulations were approximately double those in the summer simulations, despite maximum *net production rates* in the summer being approximately double those in the winter (Fig. 10d). Since buffering is generated by *depth-averaged net production* in the model, the approximately doubled maximum depth-averaged net production in winter relative to that in summer explains why maximum buffering in the winter was greater than in the summer. Similarly, the alignment of low water with nighttime respiration in

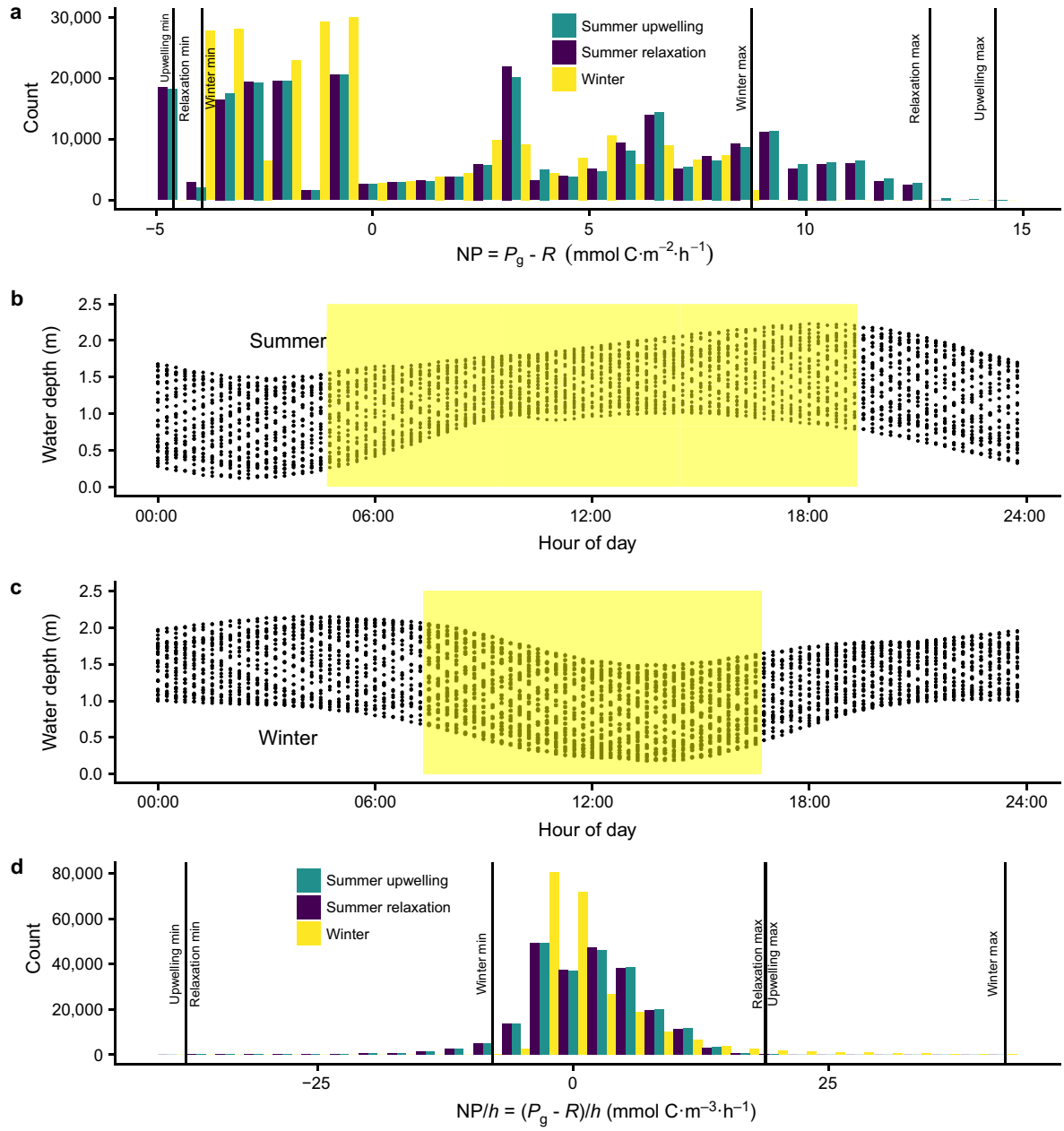

FIG. 10. (a) Histogram of all net production rates across LAI = 1–5 for all seasonal scenarios, combining fixed boundaries and side boxes model results, (b) daily cycle of water depth for the summer season, (c) daily cycle of water depth for the winter season, and (d) histogram of depth-averaged net production rates for all seasonal scenarios, combining fixed boundaries and side boxes model results. Panels b) and c) assume a mean water depth of 1.25 m, the same mean depth used in all other model runs. Yellow rectangles in panels b) and c) indicate daylight hours for summer and winter, respectively.

the summer enhanced the respiratory CO_2 flux to the water column such that the most negative depth-averaged net production in the summer was almost five times more negative than the most negative depth-averaged net production in the winter. The end result was that summer simulations demonstrated much greater potential for large negative buffering excursions (i.e., $\Delta pH < 0$) than did winter simulations.

Variation in daily cycles of water depth between summer and winter was not unique to 2016, the year in which we extracted tidal records to parameterize the model runs. We aggregated historical tidal predictions from the same tidal station and observed similar diel depth patterns as described above, which are due to the amplitude and phasing of the dominant tidal constituents in Tomales Bay (Appendix S1: Fig. S1). Together these results demonstrate that inter-seasonal tidal phasing relative to daylight can amplify or attenuate the pH range expected in a seagrass meadow. Furthermore, because this tidal phasing varies geographically as well as seasonally, pH buffering will be partially controlled by geographic location, as well as time of year and net production rates.

Discussion

The modeling analysis presented here represents an important advancement in quantifying the ability of seagrasses to buffer the effects of ocean acidification in coastal estuaries. Our approach includes key biological factors, such as plant density and seasonal variations in production and respiration, as well key physical factors, such as water depth, tidal currents, and residence time, necessary to understand and predict the buffering capacity of temperate eelgrass meadows. Our model predicts greatest pH buffering with high depth-averaged net production and residence time. Using Tomales Bay, California as a test case for the model, we found limited time-averaged buffering capability for these relatively small meadows. However, we did find short time periods where the meadow may be able to alter the pH by ± 0.2 units. The pH in the meadow was heavily dependent upon the pH of the source waters, and seasonal variability in tidal phasing relative to the diel cycle modulated pH buffering. While this model was carefully parameterized to evaluate buffering potential for Tomales Bay, we emphasize that the insights from these model experiments likely hold true for eelgrass meadows in other temperate estuaries along the west coast of North America.

Our ability to simulate localized pH buffering and draw inference from our model results depends on our ability to realistically simulate photosynthetic and respiratory rates. Duarte et al. (2010) exhaustively compiled data on worldwide observations of seagrass metabolism, including *Z. marina*. While their data do not include any measurements from the northeast Pacific, the compilation of the existing *Z. marina* data sets from the Atlantic showed average net production of approximately 0 with a range of approximately -100 to 200 $mmol \cdot m^{-2} \cdot d^{-1}$ of O_2. Assuming O_2:CO_2 equivalence (1:1), these results align well with our simulated distribution of net production rates after converting Duarte et al.'s observed rates to a per-hour basis (Fig. 10a). Eddy covariance measurements of O_2 flux in *Z. marina* meadows in the Atlantic coastal lagoons of Virginia, USA demonstrated integrated net production close to zero (metabolic balance) over ~5-d sampling periods in each of the major seasons, but also measured summer daytime peak net production rates of ~37 $mmol\ O_2 \cdot m^{-2} \cdot h^{-1}$, approximately three times as large as those in our model simulations (Rheuban et al. 2014). Winter daytime peak net production rates of 8–12 $mmol\ O_2 \cdot m^{-2} \cdot h^{-1}$ from the same study are approximately 1–1.5 times as large as the peak winter net production rates simulated in this study (Fig. 10a). These differences in production rates cannot be explained by light availability as peak solar irradiance at the top of the eelgrass canopy in both summer and winter model scenarios was greater than the light availability reaching the eelgrass canopy in the Rheuban et al. (2014) field study. However, the eddy covariance estimates included the metabolic activity of benthic macroalgae, phytoplankton and especially leaf epiphytes that were excluded from our simulations, but can combine to generate as much productivity as the *Z. marina* itself (Hemminga and Duarte 2000). Together, the results of these two observational studies are quantitatively consistent with our model calculations and support our conclusions about minimal time-averaged pH buffering estimates, but they also suggest that our model may underestimate some periods of exceptionally high pH buffering capacity resulting from daytime metabolic activity of non-eelgrass members of the community. Our conclusions about minimal time-averaged pH buffering also agree with Unsworth et al.'s (2012) empirical model of tropical seagrasses, which predicts average pH buffering of <0.02 units for seagrass meadows with residence times of 6 h.

Consideration of controls on buffering capacity

Our model was designed to evaluate the potential for a temperate eelgrass meadow to locally modify its water chemistry on hourly-to-monthly time scales. This idealized model represents one of the first attempts to understand seagrass buffering potential from a mechanistic perspective by simulating well known ecophysiological and hydrodynamic processes operating within the meadow. We return to Fig. 4 to provide a framework from which we consider our results and the processes that can lead to real-world deviations from the expected results in Tomales Bay as well as different expectations for results across estuaries. Fig. 4 showed that the ability of a seagrass meadow to buffer pH is a function of depth-averaged net production, seawater residence time within the seagrass meadow, and the pH of the source water entering the seagrass meadow. We first consider how simple model assumptions about depth-averaged net production differ from the complexity of real seagrass meadows.

Seagrass biomass.—Our model did not simulate biomass dynamics, either biomass accumulation or biomass turnover followed by subsequent export outside of the meadow. We assumed constant biomass throughout the 30-d duration of each model simulation. Accounting for biomass accumulation during certain seasons could increase the buffering capacity of the meadow, but in other seasons buffering capacity would be reduced due to seasonal dieback and decomposition in situ (equivalent to moving up or down on Fig. 4a or b). While we feel justified in our decision to

assume constant biomass over the 30-d duration of the model simulations, we recognize that deviations from this assumption will lead to different rates of P_g and R, and therefore, meadow buffering capacity. Understanding the ranges, timescales, and fate of seagrass biomass should be a priority for constraining their potential to buffer pH.

Stratification and boundary layers.—Depth-averaged net production is not only a function of the net production, but also the depth over which the photosynthetic and respiratory fluxes are averaged. In this model, we assumed a well-mixed water column over the shallow depth occupied by the meadow, which effectively generates the lower bound on the depth-averaged net production estimate by averaging the fluxes over the full depth of the water column. Our simplistic treatment of the hydrodynamics ignored water column stratification, which would reduce the volume of water over which the photosynthetic and respiratory fluxes are averaged.

The presence of a benthic boundary layer (BBL) could lead to very different carbonate chemistry within the BBL as compared to the bulk water above the BBL. However, a month-long time series in Tomales Bay in November/December 2017 showed small vertical pH gradients (typically <0.01 units), suggesting depth variation in carbonate chemistry in our study system is likely to be minor (Appendix S1: Fig. S2). It is uncertain how these pH gradients may respond to seasonal changes in environmental forcing and/or seagrass biomass. Although our model was spatially implicit (did not resolve any spatial dimension within the meadow, including depth), our low flow ($\bar{u} = -0.01$ m/s) and high flow ($\bar{u} = -0.05$ m/s) simulations essentially bounded the flow variability observed within beds (Appendix S1: Table S1). The model results show increased pH variability in the low flow conditions due to longer τ. We would expect that systems with depth gradients in velocity would experience increased pH variablity closer to the bed and dampened variability away from the bed (assuming that net primary production occurs close to the bed). Even in the low flow simulations of this study we observed limited evidence for time-averaged pH buffering, giving us confidence that inclusion of depth dynamics into the model would unlikely change the main results of this study. We also note that we did not consider the effects of strong turbulent mixing induced by wind or tides which would act to homogenize any depth gradients within the seagrass meadow.

Tidal modulation.—Depth-averaged net production can also be modulated by the tidal phasing relative to the diel cycle. Our model results predict greater maximum pH buffering in the winter when the low tides align with high solar irradiance in the afternoon. This alignment of the low tides with peak solar irradiance increases depth-averaged net production by both increasing net production (via higher light availability) and reducing the water volume over which the net photosynthetic flux is averaged. In the summer, the tidal phasing relative to the diel cycle results in a larger volume of water above the eelgrass bed in the afternoon relative to winter, effectively decreasing the depth-averaged net production by decreasing the light available for photosynthesis and increasing the volume over which any photosynthetic fluxes must be averaged. Conversely, in winter, afternoon low water promotes higher depth-averaged net production. Tidal modulation of biogeochemical dynamics in California estuaries has been previously documented. Nidzieko et al. (2014) showed that the phasing of high water at nighttime in Elkhorn Slough during spring tides created net heterotrophic conditions because the salt marsh community lining the banks could only contribute respiratory fluxes to the water since it was aerially exposed during daylight hours. Geographic and seasonal differences from those considered in the model could lead to different tidal modulations of any seagrass pH buffering. When low water aligns with daytime highs in solar irradiance and high water aligns with nighttime respiration, depth-averaged net production is amplified (move up on Fig. 4a, b). When low water aligns with nighttime peak respiration and high water occurs during the afternoons, tidal modulation decreases depth-averaged net production, and therefore, eelgrass buffering capacity.

Seawater residence time.—Residence time within the seagrass meadow is the second control on the long-term capacity of seagrass meadows to buffer pH. The residence time, τ, is a function of the seagrass meadow length and the flow velocity. We have considered a relatively small meadow in these simulations (L = 300 m), which is typical of upper Tomales Bay. The steady-state solution used to generate Fig. 4 shows that biogeochemical modification at specific net production and flow rates is a linear function of L. Larger meadows, such as those studied by Rheuban et al. (2014) covering over 1,000 ha, have longer residence times and can generate larger biogeochemical change to the overlying water (move to the right in Fig. 4a, b). For instance, Unsworth et al. (2012) also considered tropical seagrass meadows with residence times of 24 h and predicted average pH increases of up to 0.07 units in these high τ systems, much larger than those estimated for residence times of 6 h.

Vertical velocity profiles may lead to different τs within the seagrass bed compared to above it. Drag induced by the seagrass canopy will reduce flow (Fonseca et al. 1982, Nepf 2012), but drag is also likely controlled by flow velocity magnitude and direction which act to change the blade angle in the water column (Koch and Gust 1999, Nepf 2012). These effects are likely more pronounced in dense seagrass canopies. Bottom friction in rough environments may also act to reduce flow. These hydrodynamic processes highlight the possibility of interesting biological–physical feedbacks that may enhance or reduce the buffering capacity simulated in this model.

Source water.—Seagrass meadow pH is a non-linear function of the DIC and TA in the water. pH buffering in a meadow for a given amount of depth-averaged production and residence time depends on the source water being buffered since we have shown that the source waters control the average pH (Fig. 9). Lower pH waters are more sensitive to depth-averaged net production than are higher pH waters (compare Fig. 4a and b). If the pH of the source water changed, we predict that not only would the pH distribution change (Fig. 9), but so would the difference between the pH of incoming waters and those found within the meadow.

Temperature variability.—Last, our assumptions about temperature in the eelgrass meadow may lead to deviations from

our buffering capacity estimates. Low pH waters off the California coast are well known to correspond to low temperatures (<10°C; Feely et al. 2008). Waters at the mouth of west coast estuaries experience cold, low pH waters during summer months. After recently upwelled ocean water enters the estuary, it warms due to radiative forcing. Properly accounting for the balance between advective and radiative components of the heat flux requires hydrodynamic modeling tools beyond the scope of this simple model. Instead, we relied on an 8-yr observational record from Tomales Bay (Smith and Hollibaugh 1997) to reconstruct a composite annual temperature cycle in the estuary to gauge mean summer and winter temperatures. In cases where our fixed summer temperature of 18°C is an underestimate of the true temperature (e.g., summer mid-day), we are likely overestimating the buffering capacity because the temperature sensitivity for R is usually greater than the temperature sensitivity for P_g and vice-versa (although increased CO_2 availability can increase the temperature sensitivity of P_g; Zimmerman et al. 2015). Accounting for this expected temperature bias would likely dampen the net production within the eelgrass meadow, and resulting buffering capacity, within the meadow.

Next steps for future modeling.—Our model did not attempt to capture the full suite of ecological, biogeochemical, and hydrodynamic processes operating in seagrass meadows. Table 2 includes a list of many, but not all, processes which may affect seagrass meadow buffering capacity, along with their expected effects on seawater carbonate chemistry within the meadow. The processes described in Table 2 also provide an opportunity to consider the adaptability of this model to other seagrass environments. For example, calcification is likely to play a more important role in tropical seagrass meadows within coral reef ecosystems. In temperate seagrass meadows where winds are stronger, greater air-sea gas exchange may counteract local buffering by the seagrass community. In seagrass meadows adjacent to large riverine input, organic matter loading and alkalinity contributions from land-based sources are likely and should be considered. Understanding the site-specific controls on biogeochemical fluxes is critical to adapting this model to other environments. This model also only considers the metabolic activity of the *Z. marina* in the meadow alone, ignoring the contributions of periphytic algae and sedimentary metabolism to carbonate system variability. While we recognize the potential importance of both of these processes in contributing to short-term pH buffering, we did not have sufficient information to accurately characterize such spatially and temporally dynamic processes. Understanding the potential for periphytic and/or sedimentary metabolism to contribute to pH buffering on a range of timescales are important for understanding seagrass community-level buffering, but are beyond the scope of this model.

We view this modeling study as a first effort to understand localized pH buffering and ocean acidification mitigation in a temperate eelgrass meadow from a mechanistic point of view. Future efforts should incorporate the full hydrodynamic circulation using models appropriately for intertidal regions, such as TRIM (Gross and Stacey 2003), to more accurately simulate the comprehensive set of hydrodynamic and thermodynamic processes operating in the shallow coastal zone that may modulate any pH buffering. Coupling an estuarine hydrodynamic model to a more complex seagrass carbon model, such as GrassLight (Zimmerman et al. 2015) or the CSIRO seagrass model (Baird et al. 2016), would provide powerful biological–physical insights into pH buffering. These more complex modeling tools could be used to provide high spatial and temporal resolution biogeochemical projections in coastal zones and assist coastal managers' decision-making by providing scenario forecasts.

Downstream effects

Coastal ecosystem managers and stakeholders are interested not only in the buffering benefits within seagrass meadows, but also whether and how far buffering benefits extend downstream. Although we did not consider any downstream plume dynamics in this model (largely because the time-averaged ΔpH out of the box was so small), in other environments, particularly larger meadows, downstream plumes may be significant. The size and strength of the buffered plume in any coastal ecosystem (not only seagrass meadows) depends upon three factors: (1) the magnitude of the biogeochemical modification to the seawater within the meadow, (2) the balance between transport (advection) and mixing (dispersion), and (3) the water depth extending outside the seagrass meadow. Downstream plume spatial extent and intensity will increase with greater depth-averaged net production. Downstream plume intensity and along-shore extent will be maintained further downstream in environments with high along-shore advection relative to cross-shore dispersion. Cross-shore dispersion results in lateral mixing and thus dilution of the meadow's biogeochemical signature. Finally, downstream plumes will be more

Table 2. Additional processes controlling seagrass meadow carbonate chemistry not included in our model.

Process	Expected effect
Shallower water column	Increased ΔpH because more light at canopy top to support P_g
Periphyton metabolism	Increased diel pH variability from increased P_g and R
Heterotrophic metabolism in meadow (e.g., epifauna)	Decreased ΔpH due to increased R
Sedimentary metabolism	Decreased ΔpH from OM remineralization
Air/sea gas exchange	Decreased |ΔpH| because gas exchange works against biogeochemical anomalies
Significant net calcification	Increased ΔDIC and ΔTA, decreased ΔpH during daytime due to TA uptake
High (low) alkalinity fresh water input	Decreased (increased) ΔpH because source water pH is high (low)
Adjacent shoreline	Stronger downstream ΔpH plume due to limited disperion on shoreward side
Daytime oxygen production from photosynthesis	Decreased ΔpH due to increased eelgrass shoot and root respiration

easily maintained in downstream environments with similar depth ranges as the seagrass meadow. In environments with deeper water downstream of seagrass meadows, water with high pH is advected into a much larger volume of unmodified water (assuming the downstream reservoir is minimally stratified). As the two bodies of water mix, the unequal size of the buffered and non-buffered reservoirs will result in rapid dilution of any buffering effect. Therefore, stakeholders looking to benefit from any buffering effects provided by a seagrass meadow should prioritize siting their operation in shallow waters downstream of large, highly productive seagrass meadows receiving limited cross-shore mixing.

Additional ecosystem goods and services

Regardless of their potential for locally mitigating ocean acidification, seagrass meadows play many other critically important roles in coastal ecosystems, including carbon sequestration (Fourqurean et al. 2012), protection against coastal erosion and sea level rise (Duarte et al. 2013), filtration of bacterial pathogens (Lamb et al. 2017), and provision of nursery space for finfish and shellfish (Orth et al. 2006). Protecting, and where necessary, restoring seagrass meadows should be part of a portfolio of strategies for maintaining coastal ecosystem resilience for biological and human communities. The modest impact of seagrass on water chemistry may add to the already described sizable benefits of seagrass conservation and restoration.

Ocean acidification mitigation strategies

Our model has demonstrated the capacity for localized short-term pH buffering on the order of 0.1–0.2 units for small patches of seagrass meadow. This may be helpful for aquaculture or other commercial operations that can time their seawater intake to daytime periods when the seagrass meadow is locally increasing the pH. For instance, Wahl et al. (2017) observed a 40% calcification increase in the blue mussel *Mytilus edilus* with a 0.5 unit increase in pH, suggesting that buffering of up to 0.2 units could provide ~16% increases in calcification. Buffering benefits may be greater for organisms that can align the timing of their calcification with daytime increases in pH driven by seagrass or algal photosynthesis. In the same study, Wahl et al. observed that *M. edilus* shifts its calcification to daytime in treatments featuring pH variability expected under ocean acidification (lower mean pH and greater pH range) as compared to ambient pH variability, where differences in daytime vs. nighttime calcification were statistically insignificant. This work is just one example of the complexity of understanding organismal, and eventually, ecosystem responses to ocean acidification in biogeochemically variable environments.

Over longer time scales (years to decades), sustained mitigation of ocean acidification requires marine ecosystems to remove carbon from the water column and store it for extended periods of time (so-called *blue carbon*). If photosynthetic fluxes are balanced by respiration and oxidative fluxes over these longer time scales without additional long-term storage of carbon, the capacity of the ecosystem to mitigate ocean acidification will be limited.

Other short-term, targeted measures may mitigate and/or delay ocean acidification in the coastal zone. These measures may include coastal zone planning to limit land-based sources of nutrient runoff and/or low alkalinity freshwater into coastal waters, which can exacerbate ocean acidification (Strong et al. 2014), as well as planning to minimize exposure of vulnerable marine resources to locations which frequently experience acidic conditions (Boehm et al. 2015). More direct geochemical manipulation of seawater through alkalinity addition (Albright et al. 2016) and/or enhanced sea-to-air gas exchange (Koweek et al. 2016) may help with buffering against ocean acidification. Together these approaches help to define a portfolio of options which coastal communities can implement depending upon their individual needs and resources.

Drawing on this portfolio of options may help coastal communities delay the onset of ocean acidification and/or blunt its most serious consequences in the short term. However, the only long-term, global solution to ocean acidification is rapid global reduction in CO_2 emissions. Given the slow pace of efforts to reduce global CO_2 emissions, we believe that rigorous investigation of all available options for mitigating the effects of warming and acidification on marine ecosystems should be a top global scientific priority.

Acknowledgments

This work is a contribution of the Seagrass Ocean Acidification Amelioration Workshop of the Bodega Marine Laboratory, financial support for which was provided by California Sea Grant and the Coastal and Marine Sciences Institute of the University of California, Davis. Partial support for R. C. Zimmerman was provided by the National Science Foundation (Award OCE1635403). Melissa Ward contributed the data in Appendix S1: Fig. S2 of this study. We thank an anonymous reviewer and the review editor for their constructive reviews which improved this paper.

Literature Cited

Albright, R., et al. 2016. Reversal of ocean acidification enhances net coral reef calcification. Nature 531:362–365.

Baird, M. E., et al. 2016. A biophysical representation of seagrass growth for application in a complex shallow-water biogeochemical model. Ecological Modelling 325:13–27.

Barton, A., B. Hales, G. G. Waldbusser, C. Langdon, and R. A. Feely. 2012. The Pacific oyster, *Crassostrea gigas*, shows negative correlation to naturally elevated carbon dioxide levels: implications for near-term ocean acidification effects. Limnology and Oceanography 57:698–710.

Boehm, A., M. Jacobson, M. J. O'Donnell, M. Sutula, W. Wakefield, S. B. Weisberg, and E. Whiteman. 2015. Ocean acidification science needs for natural resource managers of the North American west coast. Oceanography 28:170–181.

Brewer, P. G., G. T. F. Wong, M. P. Bacon, and D. W. Spencer. 1975. An oceanic calcium problem? Earth and Planetary Science Letters 26:81–87.

Caldeira, K., and M. E. Wickett. 2003. Anthropogenic carbon and ocean pH. Nature 425:365.

Chan, F., et al. 2016. The west coast ocean acidification and hypoxia science panel: major findings, recommendations, and actions. California Ocean Science Trust, Oakland, California, USA.

Duarte, C. M., and D. Krause-Jensen. 2017. Export from seagrass meadows contributes to marine carbon sequestration. Frontiers in Marine Science 4:1–7.

Duarte, C. M., I. J. Losada, I. E. Hendriks, I. Mazarrasa, and N. Marbà. 2013. The role of coastal plant communities for climate

change mitigation and adaptation. Nature Climate Change 3:961–968.

Duarte, C. M., N. Marbà, E. Gacia, J. W. Fourqurean, J. Beggins, C. Barrón, and E. T. Apostolaki. 2010. Seagrass community metabolism: assessing the carbon sink capacity of seagrass meadows. Global Biogeochemical Cycles 24:GB4032.

Dumbauld, B. R., J. L. Ruesink, and S. S. Rumrill. 2009. The ecological role of bivalve shellfish aquaculture in the estuarine environment: a review with application to oyster and clam culture in West Coast (USA) estuaries. Aquaculture 290:196–223.

Ekstrom, J. A., et al. 2015. Vulnerability and adaptation of US shellfisheries to ocean acidification. Nature Climate Change 5:207–214.

Feely, R. A., C. L. Sabine, J. M. Hernandez-ayon, D. Ianson, and B. Hales. 2008. Evidence for upwelling of corrosive "acidified" water onto the continental shelf. Science 320:1490–1492.

Feely, R. A., et al. 2016. Chemical and biological impacts of ocean acidification along the west coast of North America. Estuarine, Coastal and Shelf Science 183:260–270.

Feng, E. Y., D. P. Keller, W. Koeve, and A. Oschlies. 2016. Could artificial ocean alkalinization protect tropical coral ecosystems from ocean acidification? Environmental Research Letters 11:074008.

Fonseca, M., J. Fisher, J. Zieman, and G. Thayer. 1982. Influence of the seagrass, *Zostera marina* L., on current flow. Estuarine, Coastal and Shelf Science 15:351–364.

Fourqurean, J. W., et al. 2012. Seagrass ecosystems as a globally significant carbon stock. Nature Geoscience 5:505–509.

Gattuso, J.-P., J.-M. Epitalon, H. Lavigne, and J. C. Orr. 2016. seacarb: Seawater carbonate chemistry. R package version 3.1.1. https://cran.r-project.org/package=seacarb

Gaylord, B., et al. 2015. Ocean acidification through the lens of ecological theory. Ecology 96:3–15.

Geyer, W. R., and P. Maccready. 2014. The estuarine circulation. Annual Review of Fluid Mechanics 46:175–197.

Green, E. P., and F. T. Short. 2003. World atlas of seagrasses. University of California Press, Berkeley, California, USA.

Gross, E. S., and M. T. Stacey. 2003. Three-dimensional hydrodynamic modeling of Tomales Bay, California. Estuarine and Coastal Modeling: 646–666.

Gruber, N., C. Hauri, Z. Lachkar, D. Loher, T. L. Frölicher, and G.-K. Plattner. 2012. Rapid progression of ocean acidification in the California Current System. Science 337:220–223.

Hearn, C. J., and J. L. Largier. 1997. The summer buoyancy dynamics of a shallow Mediterranean estuary and some effects of changing bathymetry: Tomales Bay, California. Estuarine, Coastal and Shelf Science 45:497–506.

Hemminga, M. A., and C. M. Duarte. 2000. Seagrass ecology. Cambridge University Press, Cambridge, UK.

Hönisch, B., et al. 2012. The geological record of ocean acidification. Science 335:1058–1063.

Ilyina, T., D. Wolf-Gladrow, G. Munhoven, and C. Heinze. 2013. Assessing the potential of calcium-based artificial ocean alkalinization to mitigate rising atmospheric CO_2 and ocean acidification. Geophysical Research Letters 40:5909–5914.

Invers, O., R. C. Zimmerman, R. S. Alberte, M. Pérez, and J. Romero. 2001. Inorganic carbon sources for seagrass photosynthesis: an experimental evaluation of bicarbonate use in species inhabiting temperate waters. Journal of Experimental Marine Biology and Ecology 265:203–217.

Koch, E. W., and G. Gust. 1999. Water flow in tide- and wave-dominated beds of the seagrass *Thalassia testudinum*. Marine Ecology Progress Series 184:63–72.

Koweek, D. A., D. A. Mucciarone, and R. B. Dunbar. 2016. Bubble stripping as a tool to reduce high dissolved CO_2 in coastal marine ecosystems. Environmental Science & Technology 50:3790–3797.

Kroeker, K. J., R. L. Kordas, R. N. Crim, I. E. Hendriks, L. Ramajo, G. S. Singh, C. M. Duarte, and J.-P. Gattuso. 2013. Impacts of ocean acidification on marine organisms: quantifying sensitivities and interaction with warming. Global Change Biology 19:1884–1896.

Kroeker, K. J., R. L. Kordas, R. N. Crim, and G. G. Singh. 2010. Meta-analysis reveals negative yet variable effects of ocean acidification on marine organisms. Ecology Letters 13:1419–1434.

Lamb, J. B., J. A. J. M. V. D. Water, D. G. Bourne, and C. Altier. 2017. Seagrass ecosystems reduce exposure to bacterial pathogens of humans, fishes, and invertebrates. Science 355:731–733.

Largier, J. L., C. J. Hearn, and D. B. Chadwick. 1996. Density structure in low inflow estuaries. Pages 227–241 *in* D. Aubrey and C. Friedrichs, editors. Buoyancy effects on coastal and estuarine dynamics. American Geophysical Union, Washington, D.C., USA.

Largier, J. L., J. T. Hollibaugh, and S. V. Smith. 1997. Seasonally hypersaline estuaries in Mediterranean-climate regions. Estuarine, Coastal and Shelf Science 45:789–797.

Largier, J. L., et al. 2006. WEST: a northern California study of the role of wind-driven transport in the productivity of coastal plankton communities. Deep-Sea Research Part II: Topical Studies in Oceanography 53:2833–2849.

Nepf, H. M. 2012. Flow and transport in regions with aquatic vegetation. Annual Review of Fluid Mechanics 44:123–142.

Nidzieko, N. J., J. A. Needoba, S. G. Monismith, and K. S. Johnson. 2014. Fortnightly tidal modulations affect net community production in a mesotidal estuary. Estuaries and Coasts 37:91–110.

Orth, R. J., et al. 2006. A global crisis for seagrass ecosystems. BioScience 56:987–996.

Palacios, S., and R. Zimmerman. 2007. Response of eelgrass *Zostera marina* to CO_2 enrichment: possible impacts of climate change and potential for remediation of coastal habitats. Marine Ecology Progress Series 344:1–13.

R Core Team. 2016. R: a language and environment for statistical computing. R Foundation for Statistical Computing, Vienna, Austria. www.r-project.org

Rau, G. H. 2009. Enhancing the ocean's role in CO_2 mitigation. Pages 817–824 *in* B. Freedman, editor. Global environmental change. Volume 1. Springer, Dordrecht, The Netherlands.

Rheuban, J. E., P. Berg, and K. J. McGlathery. 2014. Multiple timescale processes drive ecosystem metabolism in eelgrass (*Zostera marina*) meadows. Marine Ecology Progress Series 507:1–13.

Smith, S. V., and J. Hollibaugh. 1997. Annual cycle and interannual variability of ecosystem metabolism in a temperate climate embayment. Ecological Monographs 67:509–533.

Smith, S. V., J. T. Hollibaugh, S. J. Dollar, and S. Vink. 1991. Tomales bay metabolism: CNP stoichiometry and ecosystem heterotrophy at the land-sea interface. Estuarine, Coastal and Shelf Science 33:223–257.

Soetaert, K., T. Petzoldt, and R. W. Setzer. 2010. Solving differential equations in R: package deSolve. Journal of Statistical Software 33:1–25.

Strong, A. L., K. J. Kroeker, L. T. Teneva, L. A. Mease, and R. P. Kelly. 2014. Ocean acidification 2.0: managing our changing coastal ocean chemistry. BioScience 64:581–592.

Unsworth, R. K. F., C. J. Collier, G. M. Henderson, and L. J. McKenzie. 2012. Tropical seagrass meadows modify seawater carbon chemistry: implications for coral reefs impacted by ocean acidification. Environmental Research Letters 7:1–9.

Wahl, M., S. Schneider Covachã, V. Saderne, C. Hiebenthal, J. D. Müller, C. Pansch, and Y. Sawall. 2017. Macroalgae may mitigate ocean acidification effects on mussel calcification by increasing pH and its fluctuations. Limnology and Oceanography 63: 3–21.

Weisberg, S. B., N. Bednaršek, R. A. Feely, F. Chan, A. B. Boehm, M. Sutula, J. L. Ruesink, B. Hales, J. L. Largier, and J. A. Newton. 2016. Water quality criteria for an acidifying ocean: challenges and opportunities for improvement. Ocean & Coastal Management 126:31–41.

Wickham, H. 2009. ggplot2: elegant graphics for data analysis. Springer-Verlag, New York, New York, USA. http://ggplot2.org

Zimmerman, R. C. 2003. A biooptical model of irradiance distribution and photosynthesis in seagrass canopies. Limnology and Oceanography 48:568–585.

Zimmerman, R. C. 2006. Light and photosynthesis in seagrass meadows. Pages 303–321 *in* A. Larkum, R. J. Orth, and C. M. Duarte, editors. Seagrass: biology, ecology, and conservation. Springer, Dordrecht, The Netherlands.

Zimmerman, R. C., V. J. Hill, and C. L. Gallegos. 2015. Predicting effects of ocean warming, acidification, and water quality on Chesapeake region eelgrass. Limnology and Oceanography 60: 1781–1804.

Zimmerman, R. C., D. G. Kohrs, D. L. Steller, and R. S. Alberte. 1997. Impacts of CO_2 enrichment on productivity and light requirements of eelgrass. Plant Physiology 115:599–607.

Supporting Information

Additional supporting information may be found online at: http://onlinelibrary.wiley.com/doi/10.1002/eap.1771/full

Data Availability

Model source code necessary for reproducing the simulations presented in this study is freely available at: https://bitbucket.org/dkoweek/seagrass_box_modeling.